



# The “glacial” sapropel S6 (172 ka; MIS 6): A multiproxy approach to solve a Mediterranean “cold case”

Myers Savannah<sup>a</sup>, Rohling Eelco<sup>b,h</sup>, Donders Timme<sup>c</sup>, Grant Katharine<sup>b</sup>, Keller Jörg<sup>d</sup>, Marino Gianluca<sup>e</sup>, Sangiorgi Francesca<sup>f</sup>, Caridi Francesca<sup>a</sup>, Morigi Caterina<sup>g</sup>, Sabbatini Anna<sup>a</sup>, Negri Alessandra<sup>a,\*</sup>

<sup>a</sup> Dipartimento di Scienze della Vita e dell'Ambiente, Università Politecnica delle Marche, Via Brecce Bianche, Ancona, Italy

<sup>b</sup> Research School of Earth Science, Australian National University, 142 Mills Rd, Canberra, Australia

<sup>c</sup> Department of Physical Geography, Utrecht University, Princetonlaan 8a, Utrecht, the Netherlands

<sup>d</sup> Institut für Geo- und Umweltwissenschaften, Mineralogie und Petrologie, Albert-Ludwigs-Universität Freiburg, Albertstraße 23b, 79104 Freiburg, Germany

<sup>e</sup> Centro de Investigación Mariña, GEOMA, Palaeoclimatology Lab, Universidade de Vigo, Vigo, 3610, Spain

<sup>f</sup> Department of Earth Sciences, Utrecht University, Princetonlaan 8a, Utrecht, the Netherlands

<sup>g</sup> Dipartimento di Scienze della Terra, Università di Pisa, Via Santa Maria 53, Pisa, Italy

<sup>h</sup> Ocean and Earth Science, University of Southampton, National Oceanography Centre, Southampton, SO14 3ZH, UK

## ARTICLE INFO

Editor: M Elliot

### Keywords:

Sapropel S6  
Multiproxy approach  
Meltwater  
Monsoon  
Mediterranean Sea  
Pleistocene

## ABSTRACT

Sequences of dark, organic-rich sediment layers (sapropels) exist throughout the Neogene of the Mediterranean Sea sedimentary record. While the mechanisms behind their cyclical deposition are not entirely understood, they have been found to correspond with precession minima (Northern Hemisphere [NH] insolation maxima). This causes NH summer monsoon to shift northward and intensify, which increases precipitation over North Africa and alters Mediterranean freshwater budget, leading to restricted bottom-water ventilation and anoxia. Most Mediterranean sapropels were deposited during interglacial periods, but sapropel S6 formed during the penultimate glaciation of Marine Isotopic Stage 6 (MIS 6; 190–130 ka), during which the Eurasian ice sheet extended to its maximum size of the Quaternary. Eurasian ice-sheet melting may have provided an additional input of freshwater to the Mediterranean during S6 deposition. To test this hypothesis, we present a multiproxy paleoecological (planktic foraminifera, calcareous nannofossils, pollen, dinocysts) and geochemical (foraminiferal  $\delta^{18}\text{O}$ ) study of S6 from the Ionian Sea. We confirm that S6 deposition resulted from an interaction of two different mechanisms of freshwater input to the Mediterranean, in which: (1) local ice-sheet meltwater discharge preconditioned the basin for stratification; and (2) increased monsoon activity over North Africa caused intense precipitation and river runoff that exacerbated water-column stratification. Our results provide new evidence for the prevalence of mild/temperate and humid conditions during S6 deposition, dispelling the notion that this “glacial” sapropel formed under cold and dry conditions and we document signals of warm (interstadial) and cold (stadial) conditions within S6 in the eastern Mediterranean basin.

## 1. Introduction

Mediterranean sapropels are dark sediment layers that contain higher organic carbon concentrations than surrounding sediments (Calvert, 1983; Cita et al., 1977; Kidd, 1978; Kullenberg, 1952; Murat and Got, 1987; Olausson, 1961; Ryan and Cita, 1977; Vergnaud-Grazzini et al., 1977; Vergnaud-Grazzini, 1985). They occur (quasi) periodically

across the geological archive as far back as ~13.5 Ma during times of Northern Hemisphere [NH] summer insolation maxima concurrent with high-amplitude precession cycles (Rossignol-Strick, 1985, 1983; Rossignol-Strick et al., 1982). This specific orbital configuration increases both seasonal and land-sea temperature contrasts in the NH, intensifying NH monsoon systems (Rohling and Hilgen, 1991) as well as expanding the spatial extent of monsoon activity over north Africa (“green Sahara”

\* Corresponding author.

E-mail addresses: [s.myers@pm.univpm.it](mailto:s.myers@pm.univpm.it) (M. Savannah), [eelco.rohling@anu.edu.au](mailto:eelco.rohling@anu.edu.au) (R. Eelco), [t.h.donders@uu.nl](mailto:t.h.donders@uu.nl) (D. Timme), [katharine.grant@anu.edu.au](mailto:katharine.grant@anu.edu.au) (G. Katharine), [Joerg.Keller@minpet.uni-freiburg.de](mailto:Joerg.Keller@minpet.uni-freiburg.de) (K. Jörg), [gianluca.marino@uvigo.es](mailto:gianluca.marino@uvigo.es) (M. Gianluca), [f.sangiorgi@uu.nl](mailto:f.sangiorgi@uu.nl) (S. Francesca), [f.caridi@staff.univpm.it](mailto:f.caridi@staff.univpm.it) (C. Francesca), [caterina.morigi@unipi.it](mailto:caterina.morigi@unipi.it) (M. Caterina), [a.sabbatini@staff.univpm.it](mailto:a.sabbatini@staff.univpm.it) (S. Anna), [a.negri@staff.univpm.it](mailto:a.negri@staff.univpm.it) (N. Alessandra).

<https://doi.org/10.1016/j.palaeo.2024.112384>

Received 28 February 2024; Received in revised form 25 June 2024; Accepted 14 July 2024

Available online 18 July 2024

0031-0182/© 2024 The Authors. Published by Elsevier B.V. This is an open access article under the CC BY-NC-ND license (<http://creativecommons.org/licenses/by-nc-nd/4.0/>).

periods; GSP; Larrasoana et al., 2013; Tierney et al., 2011, 2017). This greatly enhanced freshwater drainage from the Nile River and the wider North African margin into the Mediterranean basin (Grant et al., 2022; Larrasoana et al., 2013; Osborne et al., 2008; Rohling et al., 2002). Consequently, the density structure of the Mediterranean overturning circulation (MOC) was disturbed, creating intense water column stratification that hampered deep-sea circulation and inhibited bottom water oxygenation (Cita et al., 1977; Kullenberg, 1952; Rohling, 1994; Rohling et al., 2015; Rohling and Gieskes, 1989; Ryan, 1972; Stanley et al., 1975; Thunell et al., 1977). In addition, the enhanced nutrient input into the basin causes enhanced export production and resultant biological oxygen demand in deep waters (Boyle and Lea, 1989; Calvert, 1983; Calvert et al., 1992; De Lange and Ten Haven, 1983; Nijenhuis and de Lange, 2000; Rohling, 1994; Rohling and Gieskes, 1989; Rossignol-Strick et al., 1982; Ten Haven, 1986; van Helmond et al., 2015; Zwiefel et al., 2018). Together, these oceanographic responses to enhanced freshwater influx caused basin-wide bottom water anoxia in the eastern Mediterranean Sea and, ultimately, the deposition of sapropel layers (Emeis et al., 2003; Rohling, 1994; Rohling et al., 2009, 2015). However, the more specific interplay of mechanisms behind individual sapropel formation remains debated due to regional variability of sapropels across large spatial scales, given that individual sapropel episodes vary depending on time, location, water depth of deposition, and other environmental factors (Rohling et al., 2015).

Unlike sapropels S6 and S8, which formed during glacial periods, most sapropels formed during interglacial periods (Bard et al., 2002; Rossignol-Strick, 1983; Ryan, 1972; Vergnaud-Grazzini et al., 1977). Because the previously discussed mechanisms underlying sapropel formation are more likely to occur during interglacial climates, it has been assumed that S6 and S8 formed despite adverse, cold conditions (e.g., Castradori, 1993; Emeis et al., 2003; Zirks et al., 2019).

Sapropel S6 dates from 178.5 to 165.5 ka (Konijnendijk et al., 2014; Ziegler et al., 2010), which deposited during glacial Marine Isotopic Stage (MIS) 6 (190–130 ka) (Railsback et al., 2015) when the Riss (lower latitude) and the Saalian (higher latitude) glaciations of Europe are reported, with arguably the largest Eurasian ice sheet of the Late Pleistocene (Colleoni and Liakka, 2020; Ehlers et al., 2018; Rohling et al., 2017). However, the growth of this ice sheet was punctuated by millennial-scale episodes of ice loss, as indicated by 1) accumulation of detrital material recorded in the NE Atlantic (Boswell et al., 2019; Eynaud et al., 2007; Toucanne et al., 2009), 2) smaller European ice-sheet volumes at times of maximum summer insolation (Bintanja and Van de Wal, 2008), and 3) meltwater inputs to the Black Sea (Badertscher et al., 2011; Wegwerth et al., 2020, 2019, 2014). At the same time, (Barker et al., 2019) identified the insolation peak at 173 ka (coeval with S6) as an incomplete deglaciation. Furthermore, previous studies on global (Barker et al., 2011; Cheng et al., 2016; Ding et al., 1999; Hodel et al., 2022; Marino et al., 2013; Obrochta et al., 2014; Shackleton et al., 2000) and regional (Bard et al., 2002; Bar-Matthews et al., 2003; de Abreu et al., 2003; Genty et al., 2003; Margari et al., 2010, 2014; Martrat et al., 2004, 2007; Nehme et al., 2018; Regattieri et al., 2014, 2021; Rousseau et al., 2020; Sierro and Andersen, 2022; Wainer et al., 2013; Wegwerth et al., 2020; Wilson et al., 2021) developments during MIS 6 using pollen, speleothems, alkenone-derived SSTs, foraminiferal stable isotope and trace element analyses, and ice-core records indicate pronounced millennial-scale climate variability during MIS 6 (i.e., interstadial-stadial cycles similar to those in MIS 3; (Barker et al., 2011). These millennial-scale climatological cycles are thought to relate to interactions within the ocean-atmosphere-ice sheet system (bipolar see-saw; Blunier and Brook, 2001; Broecker, 1998; Marino et al., 2013; Pedro et al., 2018; Stocker and Johnsen, 2003) with substantial impacts on the North Atlantic and Mediterranean Sea regions. Most recently, (Sierro and Andersen, 2022) (2 produced high-resolution planktic and benthic foraminiferal  $\delta^{18}\text{O}$  and  $\delta^{13}\text{C}$  records for the Iberian Margin through the penultimate glacial cycle, detailing these climate oscillations, where negative planktic foraminiferal  $\delta^{18}\text{O}$

shifts represent interstadials that align with those in the North Atlantic (Barker et al., 2011). Using their new reference record for MIS 6 millennial-scale climate variability in the North Atlantic, (Sierro and Andersen, 2022) briefly proposed that a second freshwater source in addition to North African discharge played a role in S6 deposition, namely the meltwater discharge from the Eurasian/Alpine ice-sheet through the Atlantic inflow and Rhone River inflow into the Western Mediterranean and from Po River inflow into the Eastern Mediterranean. Meltwater as a freshwater source during sapropel formation has also been suggested previously for S6 by Emeis et al. (2003); Kallel et al. (2000); Piva et al. (2008); Schmiedl et al. (1998, 2003); Thunell et al. (1983), and for other Pleistocene sapropels by Thunell and Williams (1989); Grimm et al. (2015); Grant et al. (2016); Azibeiro et al. (2021). Here we aim to 1) assess the environmental responses on the basis of high-resolution (~350 years) foraminiferal stable isotope ( $\delta^{18}\text{O}$ ) and micropaleontological (foraminifera, calcareous nannofossils, dinocysts, pollen) investigations through sapropel S6 in Ionian Sea core M25/4–12 (37°58'N, 18°11'E; 2467 m water depth), 2) shed light on the mechanisms behind the formation of “glacial” sapropel S6 by exploring the climatological and oceanographic conditions during formation, and then contribute to answer the question if meltwater input exert a substantial control on sapropel S6 deposition.

## 2. Methods

Core M25/4–12 was collected in 1993 during R/V Meteor cruise M25 Leg 4 in the Ionian Sea (37°58'N, 18°11'E) (Fig. 1), from the Calabrian slope at 2467 m water depth. The core was described in (Negri et al., 1999) and contains sapropels S1 – S10 (S2 being a missing sapropel during glacial MIS2), which span the last 330 ka, interbedded with normal bioturbated hemipelagic sediments including tephra layers Z-1 to V-4. This paper focuses on sapropel S6, recorded within core section IX (section depth 800–900 cm), as well as the surrounding sediments including the preceding core section VIII (section depth 700–800 cm). The dark intervals that we ascribe to sapropel S6 is found between 811 and 846 cm core depth and is tripartite in appearance (e.g., Blechschmidt et al., 1982; Calvert and Fontugne, 2001; Cita, 1982; Cita et al., 1977, 1984; Emeis and Party, 1996; Fontugne and Calvert, 1992; Kallel et al., 2000; Parisi and Cita, 1982; Vergnaud-Grazzini, 1985; Vergnaud-Grazzini et al., 1977); i.e., it is divided into three sections (here named, from old to young, S6a, S6b, and S6c) by two interruptions at 826.0–824.5 cm and 821.0–819.0 cm (Interruption I and Interruption II, respectively) (Fig. 2). At the base of the sapropel in section S6a, two tephra layers were visually identified (Michael Kraml, pers. comm.) at 844.5–843.5 cm and 842.5–841.5 cm (V-2 and V-0, respectively; (Keller et al., 1978; Kraml, 1997). Tephra layer V-2 is calc-alkaline and tephritic in composition with leucite and melilite, which suggests that it relates to activity in the Roman Comagmatic Province (Narcisi and Vezzoli, 1999) (See Fig. 2).

For foraminiferal, calcareous nannofossil, and stable isotope analyses (in planktic foraminifera), samples were collected every 1 cm inside the non-bioturbated sapropel and every 10 cm from bioturbated sediments outside the sapropel. For the analyses of pollen and organic-walled dinoflagellate cysts (dinocysts), the sapropel interval was sampled every 1 cm and at coarser resolution above and below it (Table 1). The sample spacing was chosen to optimize resolution within the non-bioturbated sapropel, where even the abrupt abundance variations are preserved.

### 2.1. Planktic and Benthic Foraminifera

Samples for foraminiferal analyses were dried at 60 °C, dry weighed, and washed through a 63  $\mu\text{m}$  mesh sieve. For each sample, planktic foraminiferal counts were carried out on subsamples of at least 300 individuals in the >150  $\mu\text{m}$  size fraction. This size fraction guarantees that species have reached the adult stage, and identification is most reliable

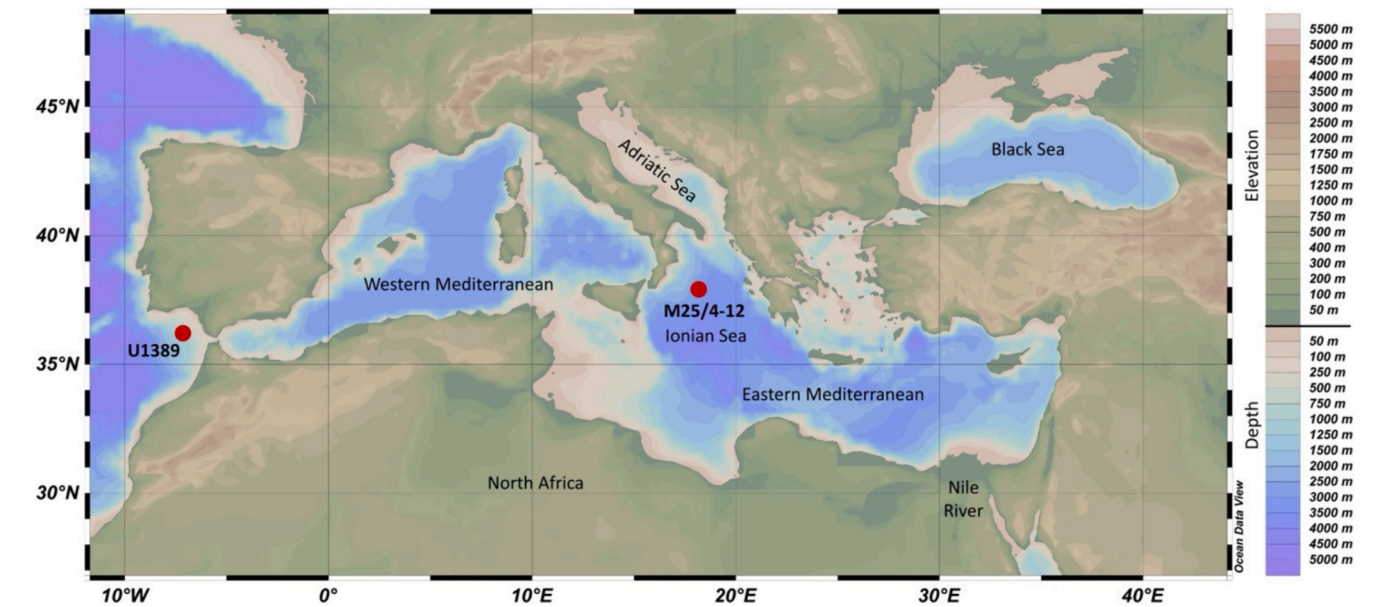


Fig. 1. Location of the M25/4-12 studied and IODP Site U1389 mentioned in this study. Figure made with Ocean Data View (Schlitzer, Reiner, Ocean Data View, <https://odv.awi.de>, 2022).

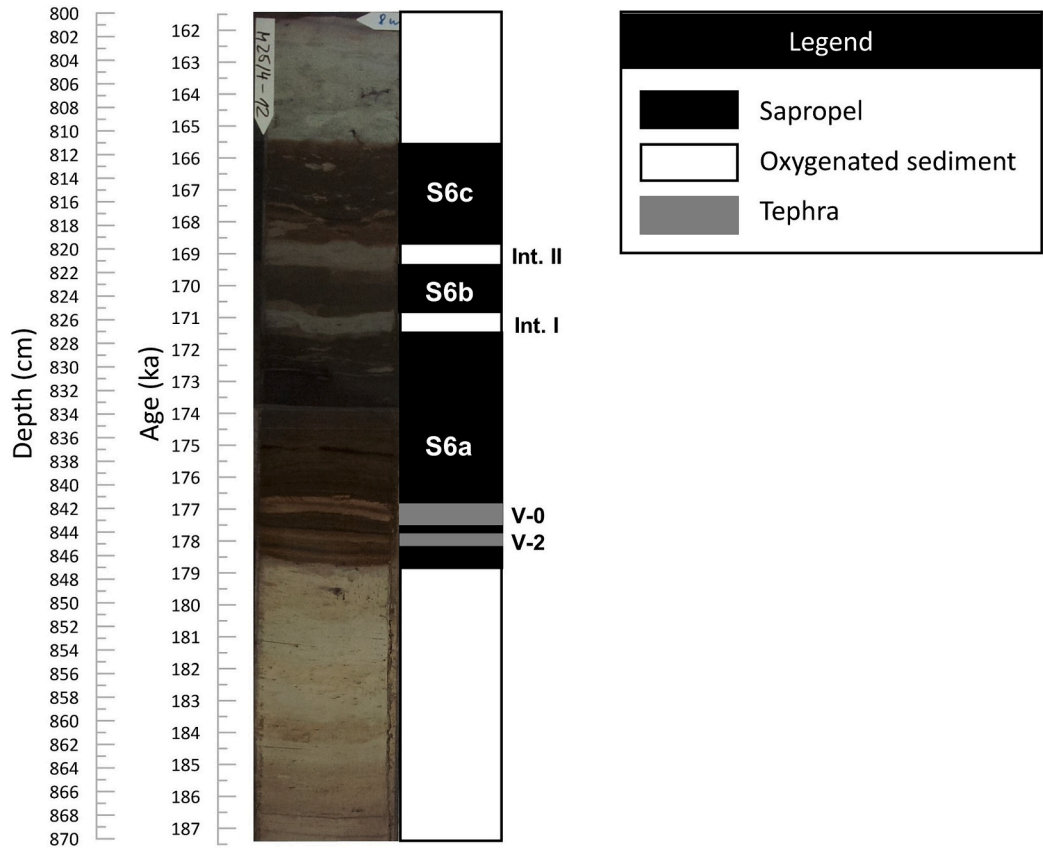


Fig. 2. Tripartite structure of sapropel S6 (S6a, S6b, S6c) including Interruptions I and II, and tephra layers V-2 and V-0, aligned with the original photo of depth 800–870 cm within Section IX from core M25/4–12 (Ionian Sea).

(Peeters et al., 1999; Sabbatini et al., 2012). Specimens were hand-picked, identified to species level, and counted. Some individuals could only be identified down to genus level (labelled “sp.” after the genus name). Only total benthic foraminiferal numbers were counted; they were not taxonomically identified. Raw counts were transformed

into absolute abundances (individual per gram sediment) and relative abundances (% relative to total planktic foraminifera counted per sample). All the data are reported in the supplementary material Table A.

Based upon ecological preferences (Rohling et al., 1993; Schiebel



**Table 1**

The sampling effort of the different proxies used in this study.

Proxy	Total number of samples	Sample Resolution (years)		Laboratory
		1-cm intervals	10-cm intervals	
Foraminifera	62	~350	~2000	Università Politecnica delle Marche
Pollen	41	~350	NA	Utrecht University
Dinocysts	41	~350	NA	Utrecht University
Calcareous Nannofossils	54	~350	~2500	Università Politecnica delle Marche
$\delta^{18}\text{O}$ ( <i>N. incompta</i> + <i>G. ruber</i> )	98	~350	~2500	Australian National University

and Hemleben, 2017) we lumped together *G. ruber alba* (white), *G. ruber ruber* (pink), *Globigerinoides conglobatus*, *Globigerinoides elongatus*, *Trilobatus sacculifer*, *Trilobatus trilobus*, *G. siphonifera*, *Globigerinella calida*, *Globoturbotalita rubescens*, and *Orbulina universa* as the warm group. *Globoturbotalita scitula*, *Neoglobobulimina pachyderma*, *Neoglobobulimina incompta*, and *Turbotalita quinqueloba* are lumped together as the cold group. Lastly, *N. dutertrei*, *Globigerinella glutinata*, *Globigerina bulloides*, and *T. quinqueloba* were grouped together as productivity-affiliated species.

We have applied the modern analogue technique (MAT; Hutson, 1980) to estimate SST variations within our record based on the planktic foraminiferal assemblage counts. We used the Mediterranean training set of (Hayes et al., 2005) considering the 10 closest analogues and using weighted averages. The distance metric was quantified using the square chord distance. The analogue package (Gavin L. Simpson) of Rstudio was used to establish the Transfer Function. Bootstrapping was not used.

## 2.2. Calcareous nannofossils

Each sample was prepared for calculation of calcareous nannofossils accumulation rates following (Flores and Sierro, 1997). Samples were assessed with a cross-polarized-light binocular microscope at 1250× magnification. For the identification we followed the taxonomy of (Young et al., 2003). At least 500 specimens were counted from random fields of view. The absolute abundance of each species/group was determined for each sample following (Flores and Sierro, 1997). Taxa were grouped into “placoliths” and “upper photic zone (UPZ)” groups following (Incarbona et al., 2011). The placoliths group includes *Gephyrocapsa* “small” (specimens whose size is < 3.5 µm) and *Emiliania huxleyi*, and is mainly driven by *Gephyrocapsa* “small”, a taxon preferential of cold water and high productivity (Gartner et al., 1987). The UPZ group includes *Syracosphaera pulchra*, *Umbellosphaera* spp., *Discosphaera tubifera*, *Rhabdosphaera clavigera*, *Rhabdosphaera stilifera*, *Oolithotus fragilis*, and *Umbilicosphaera sibogae*. All the data are reported in the supplementary material Table A.

## 2.3. Palynology: pollen and dinocysts

A total of 41 samples encompassing S6 was processed for marine and terrestrial palynology following standard methods in use at Utrecht University and based on (Wood, 1996). Sediment samples were dried in an oven at 60 °C before palynological processing. After the addition of two *Lycopodium clavatum* spore tablets (batch no. 3862, X = 9666, ± 2123 for S6) to an exact amount of dry sediment to determine palynomorph concentrations, samples were decalcified overnight using 10% hydrochloric acid (HCl). They were then decanted, rinsed with water,

and centrifuged for 5 min at 2200 rotations per minute (rpm). After decanting, silicates were removed by cold 38% hydrogen fluoride (HF) addition. Samples were placed on a shaker table for two hours at ~250 rpm to complete the reaction. Samples were then filled with water, settled overnight, centrifuged for 5 min at 2200 rpm, and decanted the day after. A surplus of 30% HCl was added to remove silicate gels. Thereafter, samples were centrifuged for 5 min at 2200 rpm, and decanted. Residues were sieved over a 250-µm mesh to remove the largest debris particles and over a 10-µm mesh and used for slide preparation with glycerin water. Two slides were made for every sample. Dinocysts and pollen and spores were identified to species level, when possible, using a light microscope at 400× magnification. Dinocyst taxonomy follows Williams et al. (2017). Pollen taxonomy follows (Beug, 1961; Reille, 1992). We lumped as “cold species” group *Spiniferites elongatus*, *Bitectatodinium tepikiense*, *Ataxiodinium choane*, and *N. labyrinthus*, and as “productivity-affiliated species group” *Bitectatodinium tepikiense* and *Brigantedinium* spp. following (Sangiorgi et al., 2003, 2002). All the data are reported in the supplementary material Table A.

## 2.4. Stable isotopes ( $\delta^{18}\text{O}$ )

Foraminiferal tests of *G. ruber* (surface dwelling species) and *N. incompta* (subsurface dwelling species previously referred to as *N. pachyderma* dextral; Rohling et al., 2004) were picked from the 300–350 and 250–300 µm size fractions, respectively, according to the methodology in (Grant et al., 2012), and analyzed for  $\delta^{18}\text{O}$ . In samples where large individuals were not available, the 250–300 µm and 200–250 µm size fractions were utilized for *G. ruber* and *N. incompta*, respectively. Between 10 and 33 specimens (average: 20) were analyzed per sample, at the Australian National University on a DELTA V mass spectrometer with Kiel IV individual acid-bath carbonate preparation line. Standards (NBS-19 and in-house Carrara marble) were run every 17 samples. Values are reported in parts per thousand (‰) relative to the V-PDB standard, and external precision is better than 0.06‰.

## 2.5. Uncertainty determination

To determine the accuracy of the assessment of the fractional abundances for each sample it is important to report the error in relation to the number of total individuals counted (Patterson and Fishbein, 1989). Error analysis of the individual sample census data (planktic foraminiferal, pollen, and organic-walled dinoflagellate cyst) of our study was performed using the standard error ( $s_{x_i}$ ) equation (eq. 1) reported by (Patterson and Fishbein, 1989), where  $x_i$  represents species abundance fraction and  $N$  represents total number of individuals. This equation has been reported to better analyze accuracy than the fractional standard deviation (Patterson and Fishbein, 1989; Wright et al., 1971). Estimates at the 1σ level were obtained.

$$s_{x_i} = [x_i(1 - x_i)/N]^{1/2} \quad (1)$$

Probabilistic analysis is performed for the various records based on uncertainties described above for the planktic foraminiferal, pollen, and organic-walled dinoflagellate cyst assemblage data and the Mean Annual Temperature (MAT) reconstructions obtained from planktic foraminiferal census counts. In addition, the analysis evaluates the uncertainties in the chronology of core M25/4–12 (see section 4). We employ a Monte Carlo approach in MATLAB (Marino et al., 2015; Rodríguez-Sanz et al., 2017; Thirumalai et al., 2016). Input data are sample ages with their 1σ uncertainties and planktic foraminiferal and palynological data with their 1σ standard errors. For each time series, individual data points are separately and randomly sampled 10,000 times within their chronological and proxy uncertainties. The chronological uncertainties are evaluated by imposing a stratigraphic constraint (monotonic increase of age with depth, analogous to (Rohling et al., 2014) to the data that are measured in a stratigraphically coherent

manner along core M25/4–12. This is done by using a random walk Monte Carlo routine that employs a Metropolis–Hastings approach to reject steps in the random walk that result in age reversals (Rodríguez-Sanz et al., 2017). Finally, each of the 10,000 time-series iterations is linearly interpolated and the probability distribution assessed at each time step, thereby determining the median (50th percentile) and the 68% (16th–84th percentile) and 95% (2.5th–97.5th percentile) probability intervals.

3. Age model

We converted depth into age for core M25/4–12 (Table 2; Fig. 3 using tie-points defined by aligning top, bottom, interruption midpoint, and midpoint depths (following the tie-points of Ziegler et al. (2010) recorded in the sedimentological core description (based on colour; Michael Kraml, pers. comm.) to the established ages used for alignment with eastern Mediterranean sapropels (ODP site 968; (Ziegler et al., 2010); Table 2). The age for each sample was then determined using linear interpolation between tie-points. The sedimentation rate for sapropel S6 in core M25/4–12 is ~2.8 cm/kyr.

Results are presented in abundance /depth plots, while the discussion will refer to time.

1σ age uncertainties were obtained through linear interpolation using age uncertainties calculated for the oxygen isotope record from Sanbao cave stalagmites reported by (Wang et al., 2008).

4. Results

Planktic foraminifera (Fig. 4) are more abundant in the middle of the sapropel layer. They are relatively well preserved in all samples and 35 taxa were identified, with *N. dutertrei* as the dominant species on average (0.2–51.4%, mean 22.6%), followed by *T. quinqueloba* (0.6–51.0%, mean 20.6%;), *N. incompta* (2.6–37.9%, mean 13.0%;), and *G. glutinata* (0.3–31.9%, mean 9.2%;). The relative abundance of the *G. ruber* group reaches its highest before the sapropel between 880.5 and 849.5 cm, is low throughout the sapropel with some small fluctuations, and then rises at the end of and after the sapropel (Fig. 4). *N. dutertrei* (Fig. 4) is absent before S6 and shows a small peak at the base. Relative abundances then gradually increase to a major peak between 843.5 and 832.5 cm, another large peak at Interruption I, and a smaller peak at Interruption II. Throughout the upper half of the sapropel S6 (828.5–810.5 cm), *N. dutertrei* percentages decrease gradually to near-absence after the sapropel. *T. quinqueloba* (Fig. 4) does not show a major relative abundance increase until 834.5 cm, from which it continues to increase to an

abundance maximum at ~830.5 cm. Then follows an overall decrease throughout the rest of the sapropel including a few small peaks, while abundances are very low after the sapropel. *Globoconella inflata* percentages only show small peaks directly before and after sapropel S6 (Fig. 4). Benthic foraminifera show small peaks only before sapropel S6, near the interruptions, and immediately after S6.

As for SST, estimates obtained by the MAT range between 10.6 and 13.5 °C (12.2 °C on average), the average standard deviation is ±0.46 °C, and the dissimilarity index (DI) is 0.48 on average.

Calcareous nannofossils are abundant (Fig. 5) and generally well preserved in all samples. *Gephyrocapsa* “small” is the dominant taxon ( $1.36 \times 10^7$ – $3.74 \times 10^7$  N/g, mean  $2.85 \times 10^7$  N/g;) followed by *Floerisphaera profunda* ( $1.10 \times 10^6$ – $1.31 \times 10^7$  N/g, mean  $6.90 \times 10^6$  N/g) and *Helicosphaera carteri* ( $4.48 \times 10^5$ – $6.91 \times 10^6$  N/g, mean  $3.21 \times 10^6$  N/g). *Coccolithus pelagicus* abundance ranges from  $1.31 \times 10^5$ – $1.81 \times 10^6$  N/g with an average of  $7.24 \times 10^5$  N/g. High *F. profunda* abundances are recorded before the sapropel until a distinct peak at ~842.5 cm, after which a gradual decrease is seen throughout the rest of the analyzed interval (Fig. 5). *H. carteri* has lower abundances before sapropel S6 but reaches a large peak at ~843.5 cm, immediately followed by a decreasing trend with fluctuations of lower values toward the top of the studied interval (Fig. 5). Finally, *C. pelagicus* abundances are high before sapropel S6, reaching a major peak ( $1.71 \times 10^6$  N/g) below the base of the sapropel at ~848.5 cm and then declining to low but almost constant values in the studied interval. Placoliths show high abundances throughout all samples, with small fluctuations. The UPZ group has high abundances before sapropel S6 and in the lower half of S6a, followed by a gradual decrease through the rest of the sapropel with some peaks at ~840 and ~827.5 cm.

In the pollen data, 18 taxa were recorded (Fig. 6). Sapropel S6 is dominated by pollen originating from trees with a mean of 75.8%, while herbs are rarer (mean 24.2%). Within the sapropel interval, deciduous *Quercus robur*-type is the dominant taxon (18.8–43.0%, mean 31.1%; Fig. 5), followed by *Pinus* (9.6–36.7%, mean 23.7%), and evergreen *Quercus* (*Q. ilex*-type and *Q. cerris*-type) (7.9–27.1%, mean 13.9%). Within the herb group, *Artemisia* is the most dominant (Fig. 6), followed by Caryophyllaceae, Chenopodiaceae, Poaceae and Cyperaceae. *Quercus* and *Pinus* abundances vary in similar ways, with relatively low and constant values throughout the sapropel. Notably, abundances of the herb taxon *Artemisia*, indicative of seasonally dry conditions, increase toward the top. Both tree and herb pollen abundances are fairly constant throughout sapropel S6, whereas a major increase occurs in tree taxa and a large decrease in herb taxa after sapropel S6, although this coincides with a large decrease in pollen concentration and count, suggesting a significant preservation bias across this transition.

A total of 20 dinocyst taxa were identified. Fig. 6 shows that, within the sapropel interval, *Spiniferites* spp. is the dominant taxon (0–61.8%, mean 28.6%), followed by *Brigantidinium* spp. (0–55.2%, mean 19.0%), *Nematosphaeropsis labyrinthus* (1.3–41.7%, mean 13.9%), and *Impagidinium aculeatum* (1.4–17.3%, mean 8.9%). *I. aculeatum* relative abundances are low and constant throughout sapropel S6, and peak after the sapropel at 800.5 cm, while absolute abundances are broadly similar but peak at 822 cm. *Lingulodinium machaerophorum* (mean 3.4%) absolute abundance peaks at the base of sapropel S6 at 841.5 cm, followed by a decrease, and then another peak at 831 cm, after which a gradual decrease occurs through the rest of sapropel S6 with minor fluctuations (Fig. 6). Both cold species and productivity-affiliated species groups show low values in the lower half of the sapropel (845–828.5 cm), transient peaks around 830 and 820 cm and higher values in the upper half of the sapropel (828.5–810.5 cm).

As for stable isotopes (Fig. 7),  $\delta^{18}\text{O}_{\text{G. ruber}}$  ranges from –1.15 to 1.95‰ and  $\delta^{18}\text{O}_{\text{N. incompta}}$  from –0.87 to 3.02‰. Both  $\delta^{18}\text{O}$  profiles follow the same general behavior with more positive values before sapropel S6 followed by a large negative excursion from ~849 cm that culminates at ~845 cm and ~839.5 ka, respectively. Thereafter, a weak trend toward positive values persists through the rest of sapropel S6,

Table 2  
Depth-Age tie-points for core M25/4–12 (Ionian Sea).

	Depth (m)	Age model (ka)
	Negri et al. (1999)	Ziegler et al. (2010)
Coretop	0.00	0
S1 (top)	0.24	6.5
S1 (bottom)	0.36	10.2
S3 (top)	4.16	77.3
S3 (bottom)	4.30	83.9
S4 (top)	5.22	99.6
S4 (bottom)	5.32	104
S5 (top)	6.04	121.4
S5 (bottom)	6.28	129.5
S6 (top)	8.11	165.5
S6 (interruption)	8.23	169.8
S6 (bottom)	8.47	178.5
S7 (top)	8.87	191.9
S7 (bottom)	9.00	198.5
S8 (top)	9.38	209.5
S8 (interruption)	9.45	213
S8 (bottom)	9.61	224.1
S9 (midpoint)	9.97	239
S10 (midpoint)	11.89	331

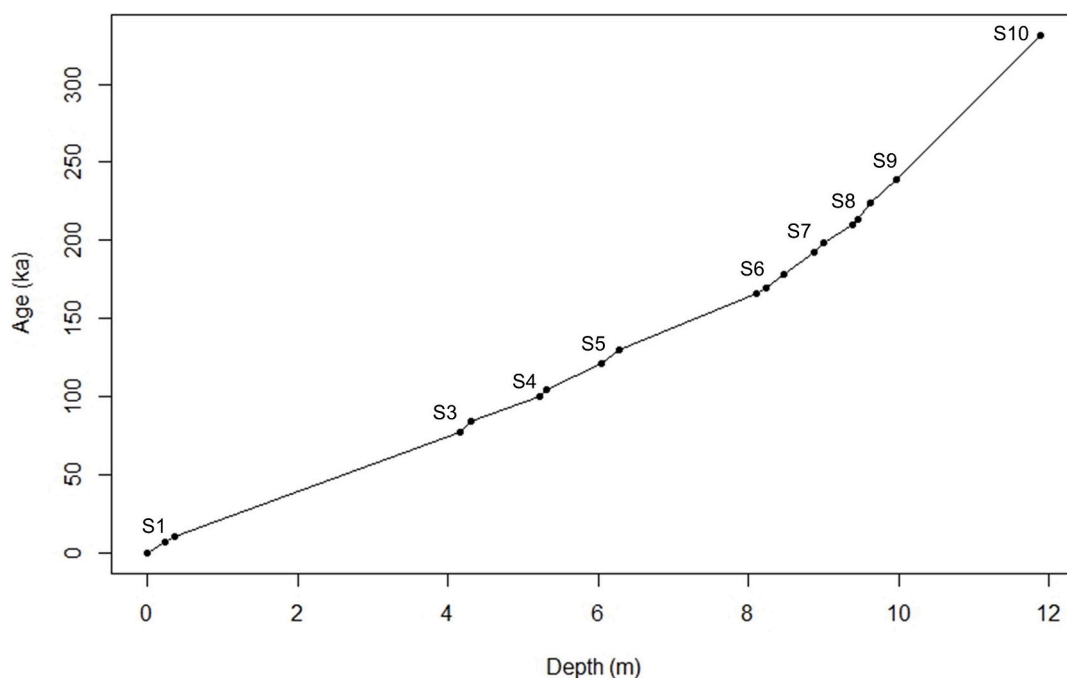


Fig. 3. Depth-to-Age conversion for Core M25/4-12 of the Ionian Sea. S = Sapropel.

with superimposed fluctuations. At the point where the visual appearance of sapropel S6 has ended, there is a particularly prominent  $\delta^{18}\text{O}_{\text{N. incompta}}$  increase.

## 5. Discussion

Sapropels deposited in response to a high versus low latitude climate interplay, that pertains to the freshwater input to the basin tied to NH ice-sheet instability (high latitudes) and NH monsoon intensification (low latitudes). A mechanism that has been previously suggested to operate in the Mediterranean region (Colleoni et al., 2012).

Our results indicate that sapropel S6 is characterized by increased primary productivity in the upper water column relative to non-sapropel intervals. This is indicated by the high percentages of productivity-affiliated foraminiferal taxa (*Neogloboquadrina dutertrei*, *Globigerinita glutinata*, *Globigerina bulloides*, and *T. quinqueloba*) (Fig. 8). Among calcareous nannofossil the Deep Chlorophyll Maximum (DCM) indicator *F. profunda* (Castradori, 1993; Negri et al., 1999; Fig. 5 and 10) shows a peak at the very base and then decreases in the remainder of the sapropel layer, while the increase of *H. carteri* suggests enhanced river input (Negri et al., 1999). Higher productivity and the development of the DCM are common features of the sapropel formation (Castradori, 1993). These are ascribed to enhanced nutrient supply due to higher, monsoon-fueled river discharge (Halim et al., 1967). In addition, they represent the hydrographic responses to buoyancy gain due to a positive shift in the basin's freshwater budget (Grelaud et al., 2012; Incarbona et al., 2022; Myers et al., 1998; Rohling and Gieskes, 1989) which is a typical characteristic of many studied sapropels (Calvert, 1983; Calvert and Pedersen, 1993; Castradori, 1993; De Lange et al., 2008; Emeis and Party, 1996; Rohling, 1994; Rohling et al., 2015; Rohling and Gieskes, 1989, among others). More surprisingly, our data suggest that temperatures were relatively mild and/or temperate during sapropel S6 ranging between 10.6 and 13.5 °C (12.2 °C on average  $\pm$  0.46 °C standard deviation), rather than prominently cold as it could be expected during a glacial period. Notably, warm water planktic foraminiferal percentages are high, although cold water taxa dominate (Fig. 8) while alkenone data indicate mean annual temperatures as low as 12 °C (Emeis et al., 2003). In this regard, *N. dutertrei* is a main faunal

component of our sapropel S6 assemblage (Fig. 4 and 8), in agreement with previous findings (Capotondi et al., 2011; Cita et al., 1977; Corselli et al., 2002; Parisi et al., 1987; Triantaphyllou et al., 2010; Violanti et al., 1991). This species is described as able to tolerate temperatures between 13 °C and 33 °C under laboratory conditions but in the natural environment is most frequent in tropical to subtropical waters, and sometimes is present in temperate waters during summer (Schiebel and Hemleben, 2017). However, in the modern Mediterranean Sea, the only higher abundances are recorded in the coldest NW area (Azibeiro et al., 2023). Also, (Toledo et al., 2007; Triantaphyllou et al., 2010) mention *N. dutertrei* as indicative of both high productivity/nutrients and milder temperatures.

This suggests that sapropel S6 deposition coincided with mild and/or temperate climate conditions and high upper water column productivity.

Our pollen record (Fig. 6 and 9) shows a clear dominance of tree taxa over herb taxa and predominance of deciduous oaks, which corroborates the existence of warm and relatively humid conditions (Wagner et al., 2019) rather than cold and arid conditions in the region of the Ionian Sea, which is further supported by a relatively low abundance of *Artemisia* (an indicator of dry environments (Donders et al., 2021; Fig. 6) especially in comparison to other glacial and interstadial sapropels (Rossignol-Strick and Paterne, 1999; Zwiep et al., 2018; Fig. 6).

The strong negative  $\delta^{18}\text{O}$  shift in our record (Fig. 7 and 10) agrees with the claim of (Emeis et al., 2003) that the onset of sapropel S6 featured among the largest negative  $\delta^{18}\text{O}$  shifts of the entire S1-S10 series, which they attribute to a strong freshwater input to the basin due to increased African monsoonal rainfall (Vergnaud-Grazzini et al., 1977). Additional evidence comes from the wider literature. For example, the speleothem stable isotope record of Soreq Cave (Israel) (Ayalon et al., 2002). indicates humid conditions throughout MIS 6, especially between 180 and 178 ka, which the authors linked to a period of African monsoon intensification (Ayalon et al., 2002). The stalagmite oxygen isotope record from Argentarola Cave (Italy) similarly indicates a humid period between 180 and 170 ka (Bard et al., 2002; Fig. 10). Also, substantially increased precipitation over Corsica is indicated during MIS6 between ~180–170 ka, by  $\delta^{18}\text{O}$  measurements from a borehole drilled in the North Tyrrhenian Sea (Toucanne et al., 2015). A

# Planktic Foraminifera

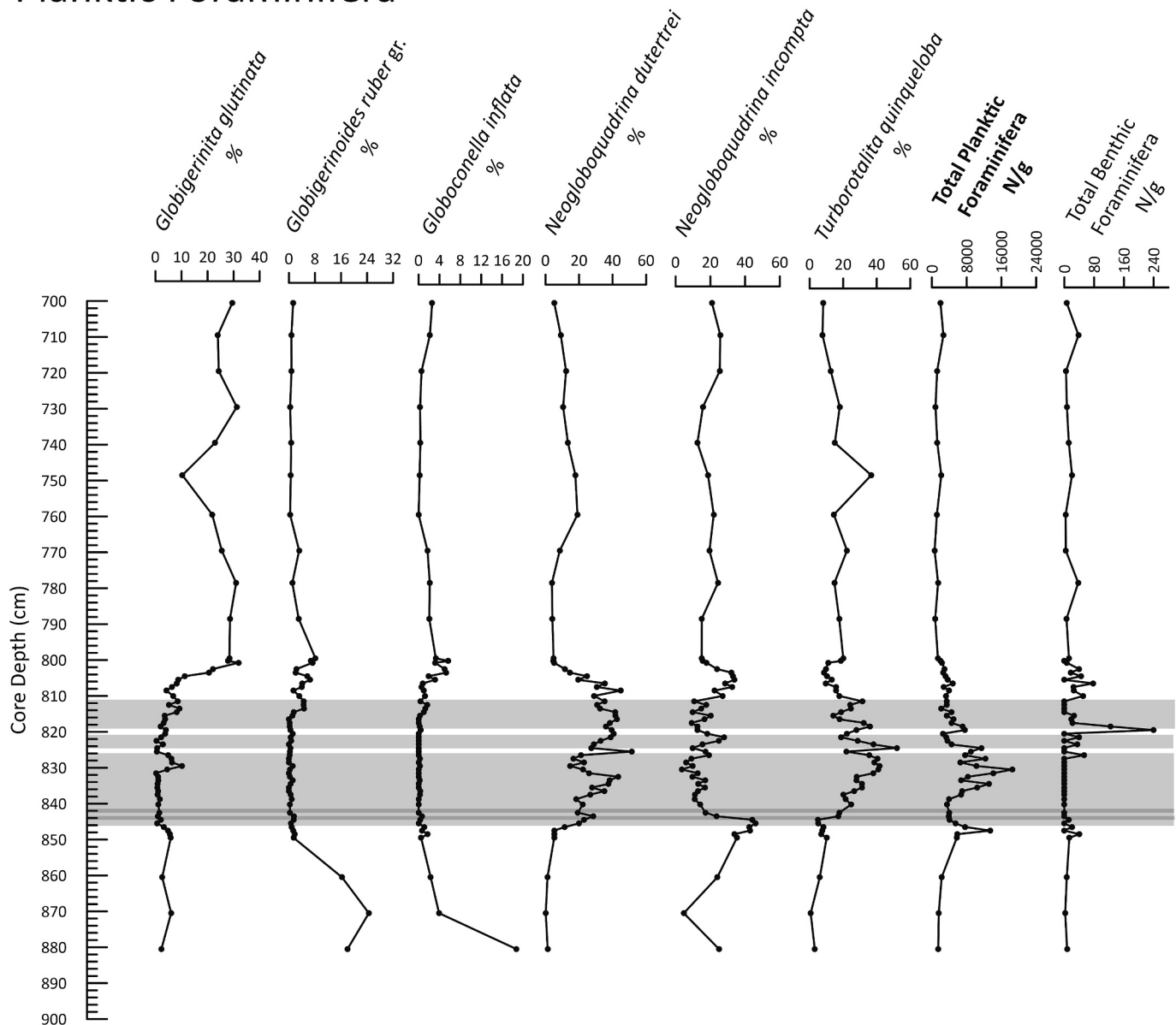


**Fig. 4.** Relative distribution (%) patterns of foraminiferal taxa and total planktic and benthic foraminifera expressed as total abundance (n°/gr) from core M25/4-12. Light grey bars represent the sapropel according to the dark intervals observed in original photo of Section IX from core M25/4-12. White bars indicate the Interruption I and II of the sapropel. Dark grey bars represent the tephra layers (V-2 and V-0).

multiproxy speleothem record of the Southern Alps has been used to infer increased cyclogenesis over the Northern Tyrrhenian Sea at 180–170 ka, resulting in wet conditions, hydrological instability, and intense precipitation (Regattieri et al., 2021). Fluctuations in tree population extent observed in Mediterranean terrestrial pollen records suggest cool and wet conditions between 185 and 155 ka (Roucoux et al., 2011) and reduced summer aridity during MIS 6e (~178–166 ka; (Margari et al., 2010). Meanwhile, speleothem hiatuses at 182.1 ka – 169.2 ka in the Piani Eterni record (Southern Alps; Columbu et al., 2018) and at 175–164 ka in the Peqiin record (Northern Israel; Bar-Matthews et al., 2003) suggest flooding of caves due to increasingly wet conditions (Regattieri et al., 2021).

The age of the above reported events coincided with an episode of African Monsoon intensification from ~179 to 165 ka (Fig. 10; Bard et al., 2002), because NH summer insolation rose toward a maximum while precession declined toward a minimum (Fig. 8). Lastly, an

increase in winter rainfall and moisture in the northern Mediterranean region has been recorded in Lake Ohrid (located between North Macedonia and Eastern Albania) for the duration of sapropel S6 (Wagner et al., 2019). Together, these observations portray a notable period of humidity/precipitation increase in the Mediterranean region during MIS 6, and particularly during sapropel S6 formation.

## 5.1. Two step nature of the sapropels S6 onset

The largest negative  $\delta^{18}\text{O}$  shift in our record marks the onset of sapropel S6 (Fig. 7 and 10). All Mediterranean sapropels show prominent, negative  $\delta^{18}\text{O}$  shifts at their onset (Calvert, 1983; Cita, 1982; Cita et al., 1977; Emeis et al., 2003; Emiliani, 1955; Fontugne and Calvert, 1992; Mangini and Schlosser, 1986; Thunell et al., 1983; Thunell and Williams, 1989; Vergnaud-Grazzini et al., 1977; Williams et al., 1978; Williams and Thunell, 1979). This feature is commonly attributed to



Calcareous Nannofossils

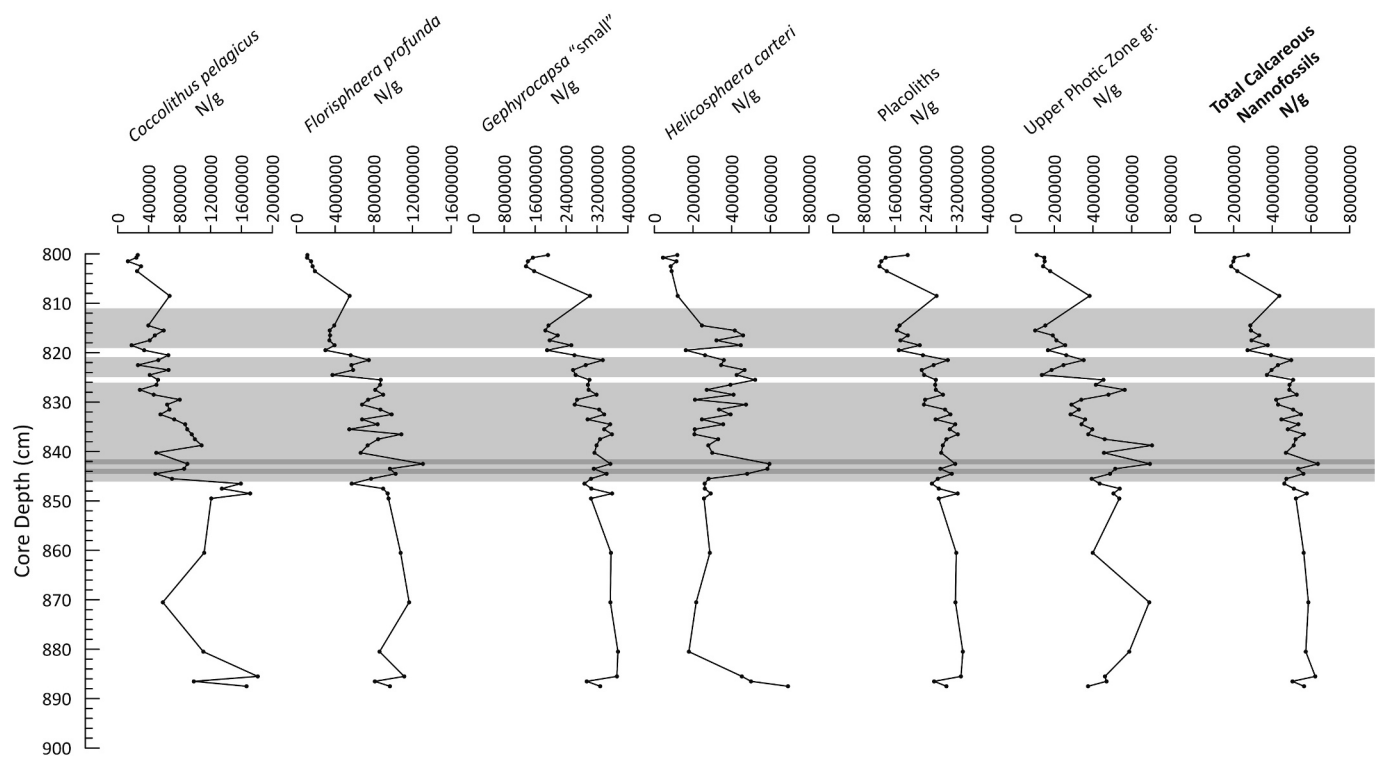


Fig. 5. Distribution patterns of calcareous nannofossil taxa collected from core M25/4-12 (Ionian Sea; this study). For sapropel legend refer to Fig. 4.

Pollen and Dinocysts

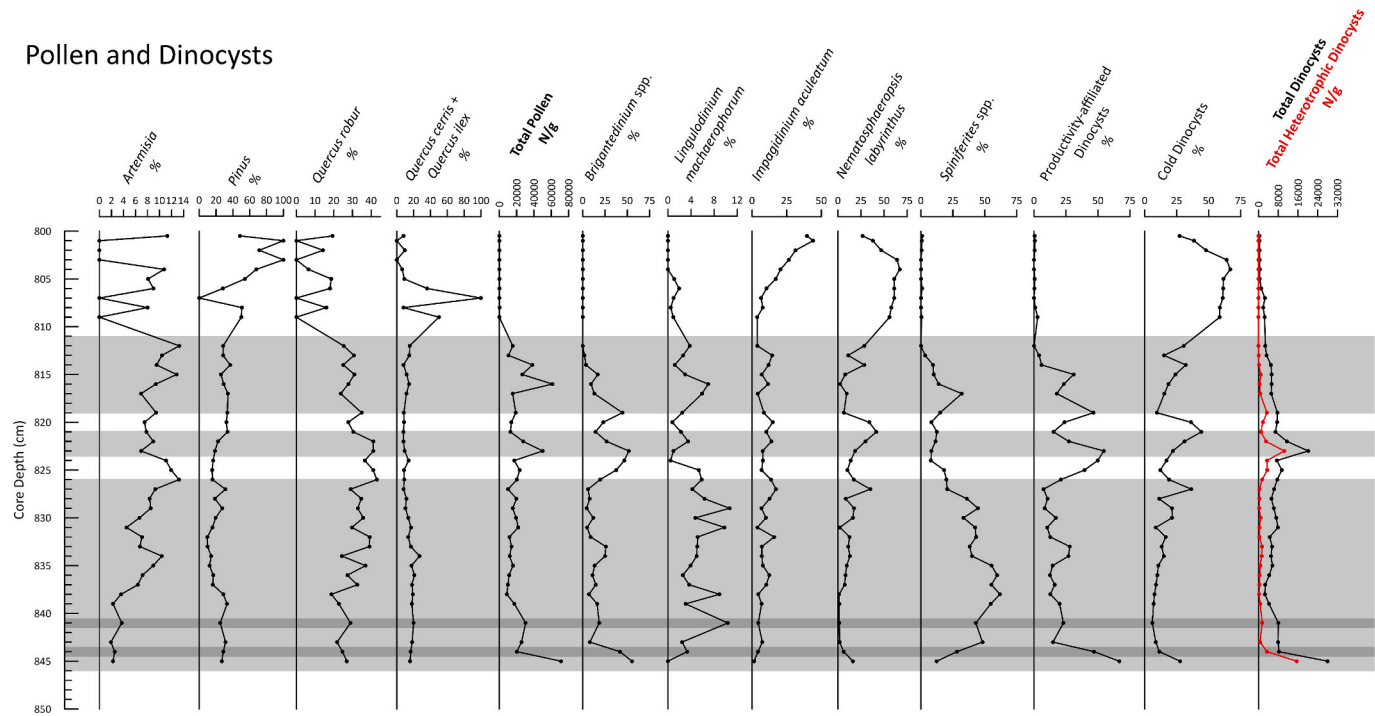


Fig. 6. Distribution patterns of pollen taxa and dinocyst taxa collected from core M25/4-12 (Ionian Sea; this study). For sapropel legend refer to Fig. 4.

monsoon-fueled freshwater input (Grant et al., 2022, 2017; Heslop et al., 2023; Osborne et al., 2008; Rohling et al., 2002; Rossignol-Strick, 1985, 1983; Rossignol-Strick et al., 1982) although the potential role of glacial meltwater input has also been discussed (Emeis et al., 2003; Kallel et al.,

2000; Piva et al., 2008; Schmiedl et al., 1998, 2003; Thunell et al., 1983).

Our high-resolution  $\delta^{18}\text{O}_{\text{G. ruber}}$  record combined with the calcareous nannofossil data exposes a two-step nature for the negative shift



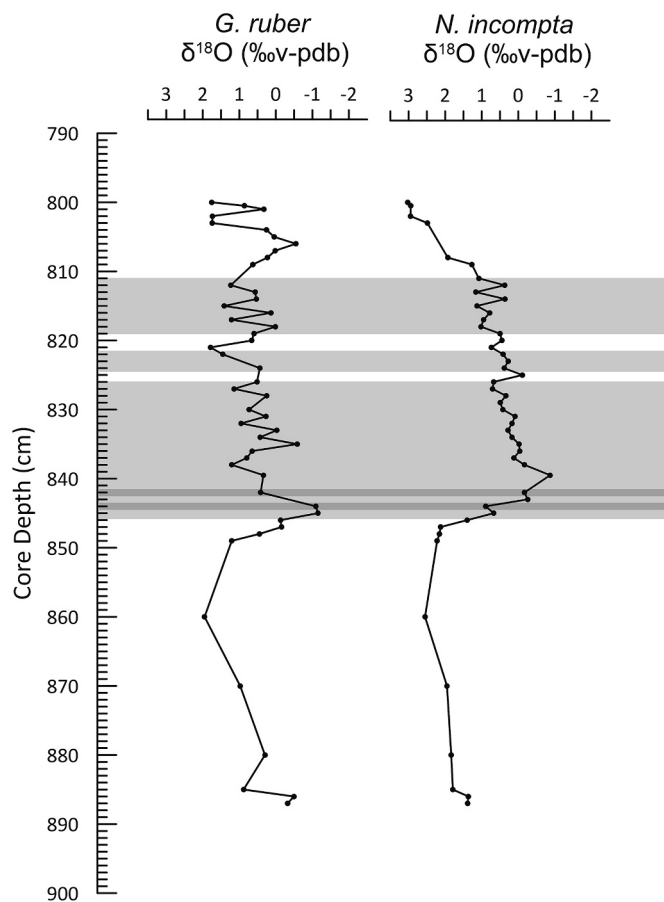


Fig. 7. Stable isotope results obtained from *G. ruber* and *N. incompta* collected from core M25/4-12 (Ionian Sea; this study). For sapropel legend refer to Fig. 4.

(freshwater input) at the sapropel S6 onset in the Ionian Sea, with a first step directly before S6 ( $\sim 178.6 \pm 0.78$  ka; arguably with a gradual onset from  $\sim 183 \pm 0.85$  ka) and a second step at the very onset of the sapropel ( $\sim 177.9 \pm 0.78$  ka; Fig. 5 and 10).

The first step coincides with a peak of cold-water, surface-dwelling foraminifera (Fig. 10), a prominent abundance peak of the calcareous nannofossil taxon *C. pelagicus* (Fig. 5 and 10), which is an indicator of colder water and high nutrient environments (Cachao and Moita, 2000; Cita et al., 1977; Negri et al., 2003; Tolderlund, 1971), and a decrease in estimated SST (Fig. 10). Furthermore, increasing values of Relative Sea Level (RSL; Grant et al., 2014) are seen before sapropel S6, in contrast to the relatively stable values recorded at its onset (Fig. 10). This suggests that the first step may represent a preconditioning freshwater input into the basin from glacial meltwater. The likely role of alpine meltwater in the formation of western Mediterranean sapropels provides additional support for this inference (Rohling et al., 2015).

The second step occurs at the sapropel S6 onset ( $\sim 177.9 \pm 0.78$  ka; Fig. 5 and 10) when *C. pelagicus* shows an abrupt decrease. The orbital configuration at this time became typical for times of monsoon intensification when precession reaches its minimum (Fig. 8; Berger and Loutre, 1991), which explains a large negative shift in *Argentarola*  $\delta^{18}\text{O}$  (Bard et al., 2002; Fig. 10). We therefore suggest that the second step in  $\delta^{18}\text{O}_{G. ruber}$  negative shift (Fig. 7 and 10) at least partly reflects increasing freshwater input due to African monsoon intensification. Yet, we consider not only freshwater input, but also temperature changes, whereby the  $\delta^{18}\text{O}_{G. ruber}$  negative shift could also (partly) indicate surface water warming. We note an absence of cold-water, surface-dwelling foraminifera at the onset of sapropel S6 (Fig. 10), while we also find an abundance increase of warmth-indicating pollen taxa (e.g., *Quercus*)

higher than expected and a coincident abundance decrease of dry, cold-indicating taxa (e.g., *Artemisia*) (Fig. 6). Moreover, dinocyst *L. machaerophorum*, associated with seasonal stratification (Sangiorgi and Donders, 2004; Zonneveld et al., 2013) peaks in abundance (Fig. 6) together with heterotrophic dinocysts indicative of riverine discharge (Dale, 2009; Limoges et al., 2013; Radi and de Vernal, 2008; Sangiorgi and Donders, 2004; Zonneveld et al., 2013). The calcareous nannofossil species, *C. pelagicus* (Fig. 10), an indicator of colder water and high nutrient levels (Andruleit, 1997; Baumann, 1995; Cachao and Moita, 2000; McIntyre and Bé, 1967; Okada and McIntyre, 1979; Raffi and Rio, 1981; Winter, 1994), was abundant during the first  $\delta^{18}\text{O}$  step, but severely decreases in abundance at the second  $\delta^{18}\text{O}$  step (Fig. 10). Also, in the same figure peaks occur in the abundances of the warm water, riverine discharge indicator *H. carteri*, (Andruleit and Rogalla, 2002; Baumann et al., 2005; Brand, 1994; Cros et al., 2000; Dimiza et al., 2014; Findlay and Giraudeau, 2002, 2000; Giraudeau, 1992; Negri et al., 1999; Triantaphyllou et al., 2009; Ziveri et al., 2004, 1995) and the Deep Chlorophyll Maximum and stratification indicator *F. profunda* (Castradori, 1993; Negri et al., 1999) (Fig. 10). and the increased nutrient and riverine discharge indicating (Fig. 5 k). Similar abundance peaks have been noted for these calcareous nannofossil taxa in other cores (Libyan Sea, Triantaphyllou et al., 2010; Ionian/Libyan Sea, Castradori, 1993). Hence, we argue that the second  $\delta^{18}\text{O}$  step at the sapropel S6 onset represents both an increase in monsoon freshwater input and surface water warming.

Overall, we infer a two-step mechanism for the formation of S6, comprising (1) ice-sheet instability that caused local meltwater events, which preconditioned the basin for stratification, followed by (2) African monsoon intensification that increased precipitation and river runoff, with concomitant (surface water) warming, which accelerated water-column stratification.

## 5.2. Sapropel S6 interruptions

Sapropel interruptions (generally characterized by transient benthic foraminiferal repopulations) occur not only in sapropel S6 but also in other sapropels, such as S1, and are related to weakened monsoon influences and/or cooling (Abu-Zied et al., 2008; Mercone et al., 2001; Rohling et al., 1993, 2015; Rohling and Pälike, 2005). Also, atmospheric variability has been demonstrated an integral feature of the system (Dirksen and Meijer, 2020). The youngest half of sapropel S6, which contains both interruptions, bears relatively low warm-water foraminiferal relative abundances and high cold-water foraminiferal (Fig. 8 Fig. 10) and dinocyst abundances (Fig. 9). Together, these features indicate colder temperatures relative to the older part of sapropel S6, in apparent agreement with the summer insolation (Fig. 8; Berger and Loutre, 1991 and RSL decrease (Fig. 10; Grant et al., 2014). Schmiedl et al. (2003) argued that slight coolings during deposition of the younger half of sapropel S6 would have sufficed to disrupt water-column stratification, leading to deep-sea ventilation events, in contrast to sustained stratification during deposition of the older half of the sapropel, which formed under warmer conditions. Similar to the interruption in S1, the sapropel S6 interruptions are marked by reappearance of benthic foraminifera (Fig. 4) reflecting bottom-water reventilation associated with the cooling events (Casford et al., 2003; Jorissen, 1999).

## 5.3. Millennial-scale climate variability during sapropel S6

(Sierro and Andersen, 2022) provide evidence that millennial-scale climate variability and associated warming events affected the North Atlantic, including the Iberian Margin, during sapropel S6 deposition, and that this also affected the Eastern Mediterranean basin. Unlike the variability seen in our  $\delta^{18}\text{O}_{G. ruber}$  record (Fig. 7 and 10), our  $\delta^{18}\text{O}_{N. incompta}$  (subsurface species; Fig. 7 and 10) shows only a general negative “bell” shape curve, with major shifts only at the onset and the termination of sapropel S6. Given that  $\delta^{18}\text{O}_{N. incompta}$  changes

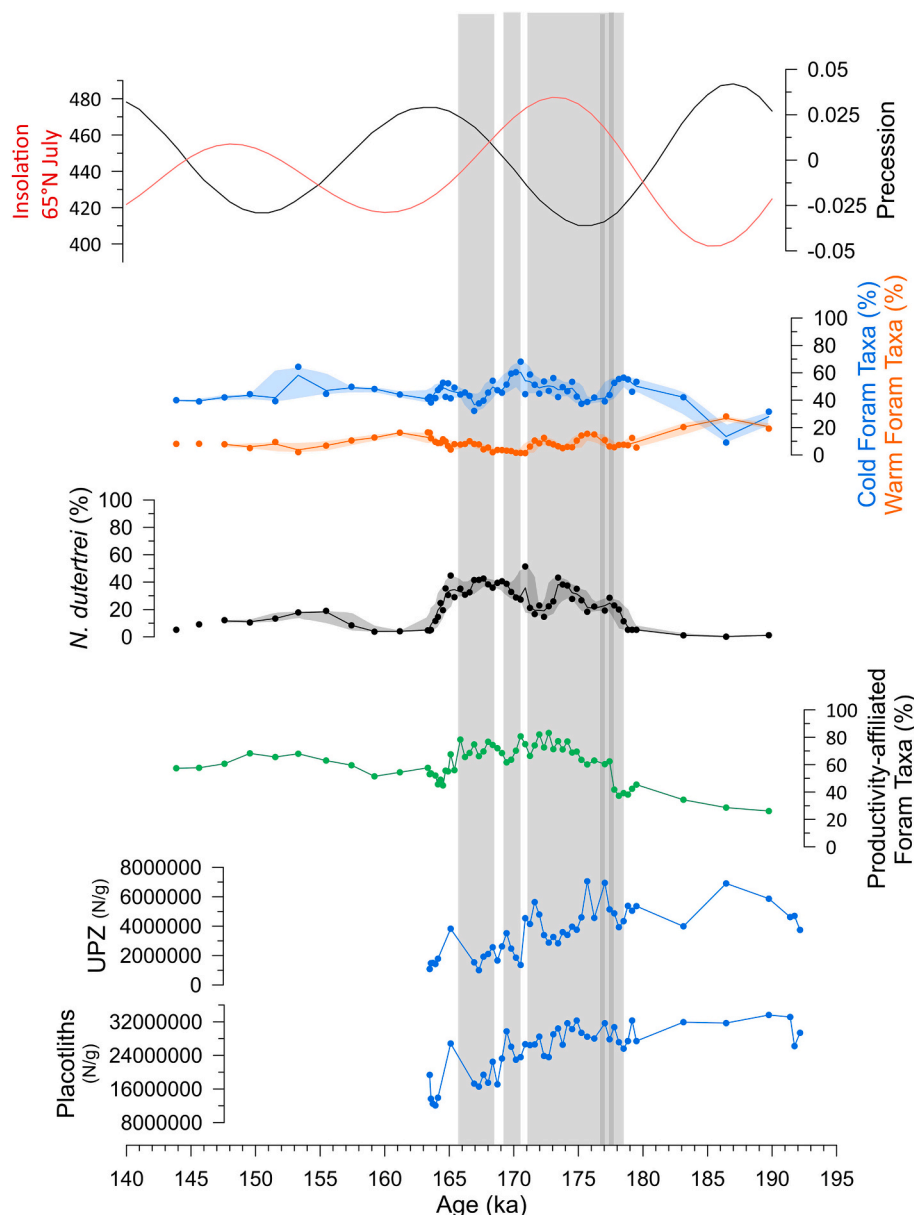


**Fig. 8.** Distribution of placoliths, upper photic zone (UPZ) calcareous nannofossils, *N. dutertrei*, cold foraminifera taxa, warm foraminifera taxa and productivity affiliated foraminifera in the studied interval compared with Northern Hemisphere summer insolation (65°N July; W/m<sup>2</sup>; red) and precession (Berger and Loutre, 1991), and). Dots represent the recorded relative abundance (%). Shaded areas represent the 95% probability interval. Solid lines represent the probability median (50%). For sapropel legend refer to Fig. 4. (For interpretation of the references to colour in this figure legend, the reader is referred to the web version of this article.)

predominantly in a volumetrically attenuated manner from freshwater-induced surface water  $\delta^{18}\text{O}$  perturbations with some winter-cooling overprint (Rohling et al., 2014), we infer that the strong  $\delta^{18}\text{O}_{\text{G. ruber}}$  variability (relative to  $\delta^{18}\text{O}_{\text{N. incompta}}$ ) resulted mainly from superimposed surface water temperature changes during the warm season, with limited impact on winter/subsurface temperatures. We graphically correlate the three most negative values of  $\delta^{18}\text{O}_{\text{G. ruber}}$  from our record with prominent warming events 6i, 6iii, and 6iv described by (Sierro and Andersen, 2022) (Fig. 10). Accordingly, the positive shifts of  $\delta^{18}\text{O}_{\text{G. ruber}}$  likely represent cold spells in between the warming events. These temperature fluctuations seem to have been most notable in the warm seasons (affecting only  $\delta^{18}\text{O}_{\text{G. ruber}}$ ). However, it cannot be excluded that these fluctuations can correlate also to salinity changes as the increased runoff signal (Log Ti/Ca in (Hodell et al., 2015) at the Iberian margin suggests.

#### 5.4. The end of sapropel S6 and the recovery to oxygenated conditions

The recovery to oxygenated bottom water conditions corresponded a resumption of deep-water formation and associated basin-wide water column re-oxygenation (De Lange et al., 2008; Reed et al., 2011; Reitz et al., 2006; Van Santvoort et al., 1996). There is a rich literature about this for S1, using different proxies (De Lange et al., 2008; Filippidi and De Lange, 2019; Jorissen et al., 1993; Rohling et al., 1997; Schmiedl et al., 2010; Tachikawa et al., 2015; van Helmond et al., 2015). Our stable isotope results shed light on this matter for sapropel S6. As discussed above,  $\delta^{18}\text{O}_{\text{N. incompta}}$  (Fig. 10) is more likely to be impacted by major forcing that could substantially affect the subsurface, which was dominated by freshwater influences (Rohling et al., 2004). A key feature detailed by our  $\delta^{18}\text{O}_{\text{N. incompta}}$  is the sharp, abrupt increase precisely at the end of the visible sapropel S6 expression (Fig. 10). This marks the end of significant freshwater influx (Fontugne and Calvert, 1992; Kallel

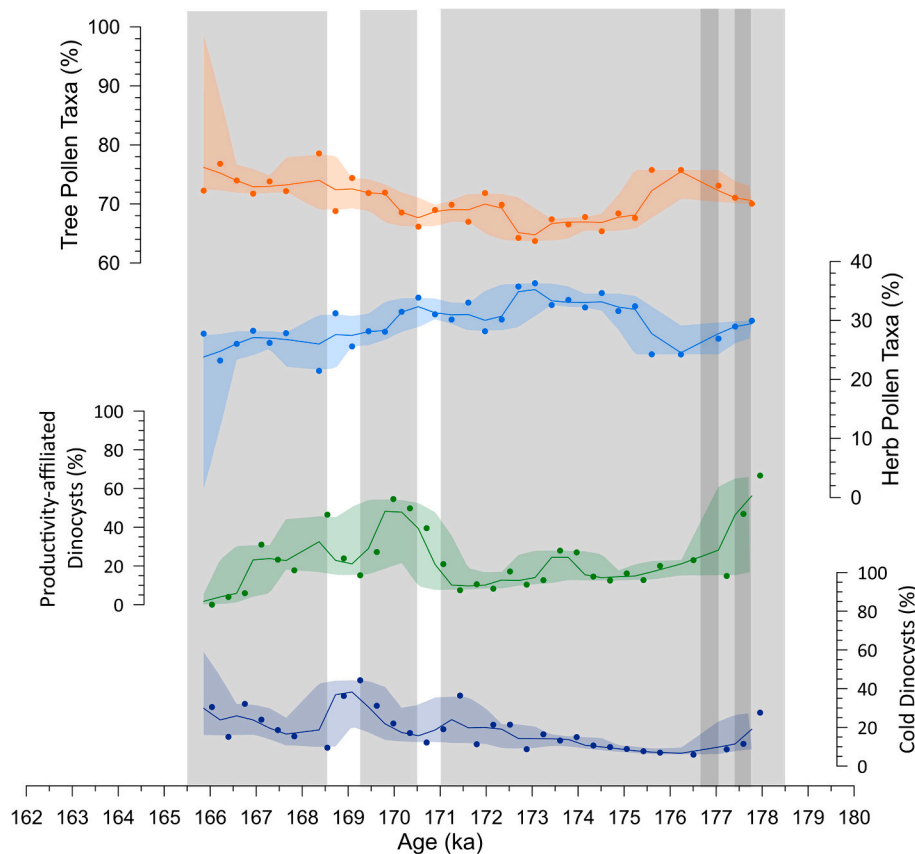


**Fig. 9.** Summary of palynological assemblage collected from core M25/4–12 (Ionian Sea; this study). Dots represent the recorded relative abundance (%). Shaded areas represent the 95% probability interval. Solid lines represent the probability median (50%). For sapropel legend refer to Fig. 4.

et al., 1997, 2000; Rohling et al., 2004; Thunell and Williams, 1989; Vergnaud-Grazzini et al., 1977) from monsoon activity and/or glacial meltwater. It also coincides with reappearance of benthic foraminifera (Fig. 9???) and the planktic species *G. inflata* (Fig. 4), both indicators of deep ventilation/mixing (Rohling, 1999; Van Straaten, 1972; Van Straaten, 1966). Additionally, the orbital configuration conducive of sapropel deposition gradually changed to conditions less favorable for sapropel deposition by the end of sapropel S6, which arguably weakened monsoonal activity, decreasing freshwater influx (Fig. 8). This is further supported by a concomitant decrease in Asian monsoon activity marked by an abrupt positive shift in Argentarola speleothem  $\delta^{18}\text{O}$  (Fig. 10; Bard et al., 2002). Together, these observations imply a reduction in water column stratification, which facilitated deep convection and consequent bottom water re-oxygenation.

## 6. Conclusion

Glacial sapropels have traditionally received less attention than those deposited during interglacial periods, which are generally more intensively developed. We apply a high-resolution, multiproxy approach to investigate sapropel S6 that deposited during glacial Marine Isotope Stage 6. Our dataset indicates that sapropel S6 was deposited in response to a high versus low latitude climate interplay that has been previously suggested to operate in the Mediterranean region. This interplay pertains to the freshwater input to the basin tied to NH ice-sheet instability (high latitudes) and NH monsoon intensification (low latitudes). We find that these processes resulted in two mechanisms that led to S6 formation: (1) Eurasian/Alpine ice sheet meltwater input that preconditioned the basin for stratification; followed by (2) increased monsoon runoff that intensified stratification. We also observe distinct signals of millennial-scale climate variability in  $\delta^{18}\text{O}_{\text{G. ruber}}$  within the Ionian Sea

during the sapropel S6 deposition, which can be related to widespread stadial-interstadial cycles.

During S6 deposition, the Mediterranean region experienced a mild/temperate climate with humid conditions, which are contrasted with the notion glacial periods in this region feature cold and dry climates. Cooling is apparent through the second half of the sapropel, which helps to explain the presence of deep water re-ventilation events (sapropel interruptions). Finally, we observe that the end of the sapropel S6 deposition coincided with a sharp termination of the freshwater inputs to the basin.

## CRediT authorship contribution statement

**Myers Savannah:** Writing – review & editing, Writing – original draft, Visualization, Investigation, Conceptualization. **Rohling Eelco:** Writing – review & editing, Conceptualization. **Donders Timme:** Writing – review & editing, Investigation. **Grant Katharine:** Writing – review & editing, Investigation. **Keller Jörg:** Conceptualization. **Marino Gianluca:** Writing – review & editing, Methodology, Formal analysis, Conceptualization. **Caridi Francesca:** Writing – review & editing, Investigation. **Morigi Caterina:** Writing – review & editing, Investigation. **Sabbatini Anna:** Writing – review & editing, Investigation. **Negri Alessandra:** Writing – review & editing, Writing – original draft, Visualization, Investigation, Conceptualization.

## Declaration of generative AI and AI-assisted technologies in the writing process

During the preparation of this work the author(s) used ChatGPT in order to improve language. After using this tool/service, the author(s) reviewed and edited the content as needed and take(s) full responsibility

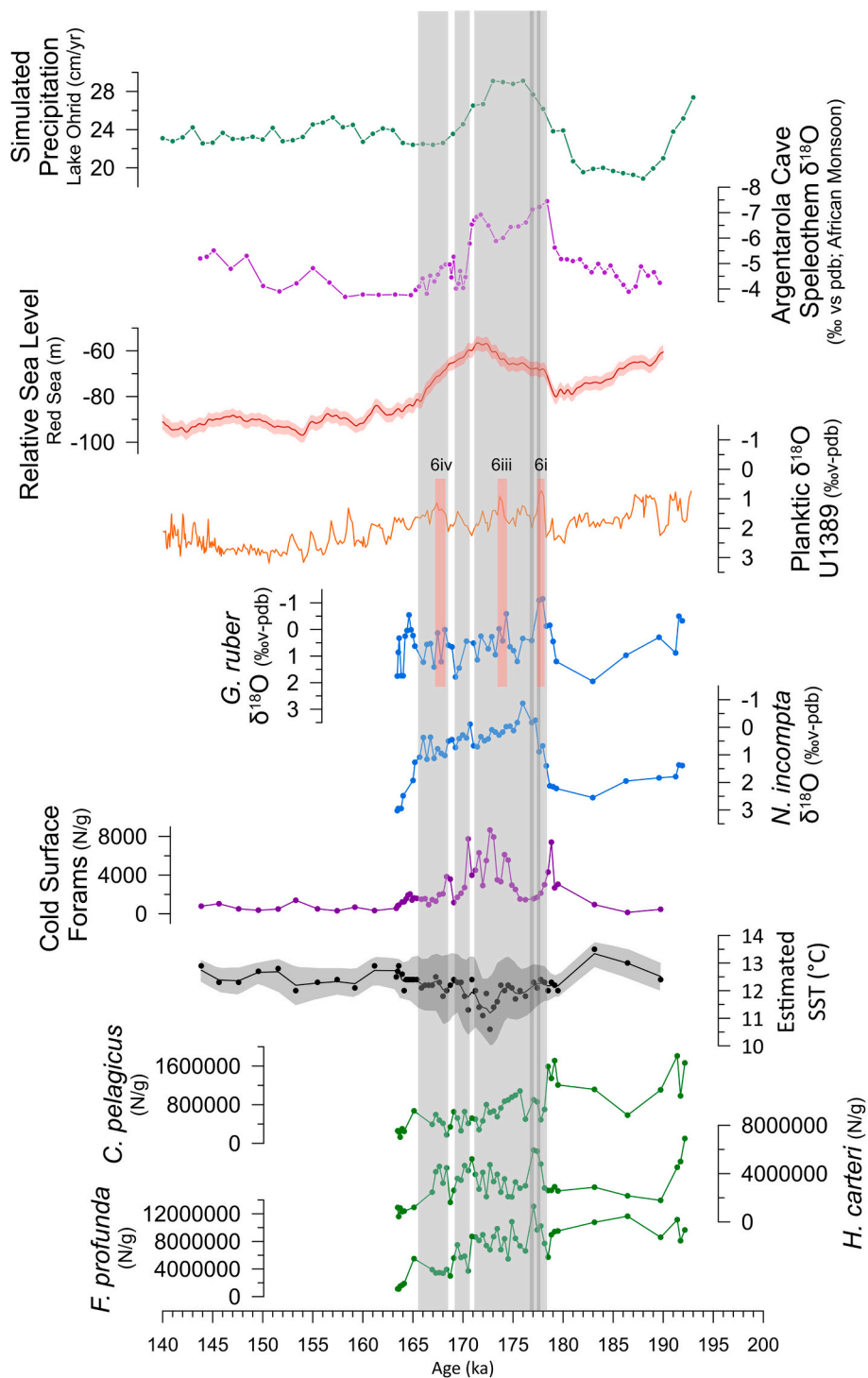


**Fig. 10.** Absolute abundances of noteworthy calcareous nannofossils: *C. pelagicus*, *H. carteri*, and *F. profunda*, respectively; SST estimated using MAT; Summation of cold-water, surface-dwelling planktic foraminiferal taxa abundances (*T. quinqueloba*, *N. pachyderma*, *N. incompta*, *G. scitula*);  $\delta^{18}\text{O}_{N. incompta}$  (Ionian Sea; this study);  $\delta^{18}\text{O}_{G. ruber}$  (Ionian Sea; this study); Orange bars represent warming events 6i, 6ii, 6iii, and 6iv (Sierro and Andersen, 2022);  $\delta^{18}\text{O}_{G. bulloides}$  (U1389; Sierro and Andersen, 2022); Relative Sea Level (probability maximum, red line; 95% probability interval, red shading; Grant et al., 2014); Argentarola Cave Speleothem  $\delta^{18}\text{O}$  (Bard et al., 2002); For sapropel legend refer to Fig. 4. (For interpretation of the references to colour in this figure legend, the reader is referred to the web version of this article.)

for the content of the publication.

**Declaration of competing interest**

The authors declare that they have no known competing financial interests or personal relationships that could have appeared to influence

the work reported in this paper.

**Data availability**

Data are in supplementary A and B



## Acknowledgments

The research benefited from the DISVA Department funds 2023 to Alessandra Negri. It is part of the PhD Fellowship awarded to Savannah Myers. We are deeply indebted to Laura Aiudi and Michelle de Groot for the nannofossil and palynomorphs data obtained in their Master thesis. We are grateful to the reviewers for their useful comments that helped us to improve the manuscript.

## Appendix A. Supplementary data

Supplementary data to this article can be found online at <https://doi.org/10.1016/j.palaeo.2024.112384>.

## References

- Abu-Zied, R.H., Rohling, E.J., Jorissen, F.J., Fontanier, C., Casford, J.S., Cooke, S., 2008. Benthic foraminiferal response to changes in bottom-water oxygenation and organic carbon flux in the eastern Mediterranean during LGM to recent times. *Mar. Micropaleontol.* 67, 46–68. <https://doi.org/10.1016/j.marmicro.2007.08.006>.
- Andrúleit, H., 1997. Coccolithophore fluxes in the Norwegian-Greenland Sea: seasonality and assemblage alterations. *Mar. Micropaleontol.* 31, 45–64. [https://doi.org/10.1016/S0377-8398\(96\)00055-2](https://doi.org/10.1016/S0377-8398(96)00055-2).
- Andrúleit, H., Rogalla, U., 2002. Coccolithophores in surface sediments of the Arabian Sea in relation to environmental gradients in surface waters. *Mar. Geol.* 186, 505–526. [https://doi.org/10.1016/S0025-3227\(02\)00312-2](https://doi.org/10.1016/S0025-3227(02)00312-2).
- Ayalon, A., Bar-Matthews, M., Kaufman, A., 2002. Climatic conditions during marine oxygen isotope stage 6 in the eastern Mediterranean region from the isotopic composition of speleothems of Soreq Cave, Israel. *Geology* 30, 303–306. [https://doi.org/10.1130/0091-7613\(2002\)030<0303:CCDMOI>2.0.CO;2](https://doi.org/10.1130/0091-7613(2002)030<0303:CCDMOI>2.0.CO;2).
- Azibeiro, L.A., Sierro, F.J., Capotondi, L., Lirer, F., Andersen, N., González-Lanchas, A., Alonso-García, M., Flores, J.-A., Cortina, A., Grimalt, J.O., 2021. Meltwater flux from northern ice-sheets to the Mediterranean during MIS 12. *Quat. Sci. Rev.* 268, 107108. <https://doi.org/10.1016/j.quascirev.2021.107108>.
- Azibeiro, L.A., Kučera, M., Jonkers, L., Cloke-Hayes, A., Sierro, F.J., 2023. Nutrients and hydrography explain the composition of recent Mediterranean planktonic foraminiferal assemblages. *Mar. Micropaleontol.* 179, 102201. <https://doi.org/10.1016/j.marmicro.2022.102201>.
- Badertscher, S., Fleitmann, D., Cheng, H., Edwards, R.L., Göktürk, O.M., Zumbühl, A., Leuenberger, M., Tüysüz, O., 2011. Pleistocene water intrusions from the Mediterranean and Caspian seas into the Black Sea. *Nat. Geosci.* 4, 236–239. <https://doi.org/10.1038/ngeo1106>.
- Bard, E., Delaygue, G., Rostek, F., Antonioli, F., Silenzi, S., Schrag, D.P., 2002. Hydrological conditions over the western Mediterranean basin during the deposition of the cold Sapropel 6 (ca. 175 kyr BP). *Earth Planet. Sci. Lett.* 202, 481–494. [https://doi.org/10.1016/S0012-821X\(02\)00788-4](https://doi.org/10.1016/S0012-821X(02)00788-4).
- Barker, S., Knorr, G., Edwards, R.L., Parrenin, F., Putnam, A.E., Skinner, L.C., Wolff, E., Ziegler, M., 2011. 800,000 years of abrupt climate Variability. *Science* 334, 347–351. <https://doi.org/10.1126/science.1203580>.
- Barker, S., Knorr, G., Conn, S., Lordsmith, S., Newman, D., Thornalley, D., 2019. Early Interglacial Legacy of Deglacial climate Instability. *Paleoceanog. Paleoclimatol.* 34, 1455–1475. <https://doi.org/10.1029/2019PA003661>.
- Bar-Matthews, M., Ayalon, A., Gilmour, M., Matthews, A., Hawkesworth, C.J., 2003. Sea-land oxygen isotopic relationships from planktonic foraminifera and speleothems in the Eastern Mediterranean region and their implication for paleorainfall during interglacial intervals. *Geochim. Cosmochim. Acta* 67, 3181–3199. [https://doi.org/10.1016/S0016-7037\(02\)01031-1](https://doi.org/10.1016/S0016-7037(02)01031-1).
- Baumann, K.H., 1995. Morphometry of Quaternary Coccolithus pelagicus coccoliths from Northern North Atlantic and its paleoceanographical significance. In: *5th INA Conference in Salamanca Proceedings*, pp. 11–21.
- Baumann, K.-H., Andrúleit, H., Böckel, B., Geisen, M., Kinkel, H., 2005. The significance of extant coccolithophores as indicators of ocean water masses, surface water temperature, and palaeoproductivity: a review. *Paläontol. Z.* 79, 93–112. <https://doi.org/10.1007/BF03021756>.
- Berger, A., Loutre, M.-F., 1991. Insolation values for the climate of the last 10 million years. *Quat. Sci. Rev.* 10, 297–317.
- Beug, H.-J., 1961. Leitfaden der Pollenbestimmung für Mitteleuropa und angrenzende Gebiete (No Title).
- Bintanja, R., Van de Wal, R.S.W., 2008. North American ice-sheet dynamics and the onset of 100,000-year glacial cycles. *Nature* 454, 869–872. <https://doi.org/10.1038/nature07158>.
- Bleischmidt, G., Cita, M.B., Mazzei, R., Salvatorini, G., 1982. Stratigraphy of the western Mediterranean and southern Calabrian ridges, eastern Mediterranean. *Mar. Micropaleontol.* 7, 101–132.
- Blunier, T., Brook, E.J., 2001. Timing of Millennial-Scale climate Change in Antarctica and Greenland during the last Glacial Period. *Science* 291, 109–112. <https://doi.org/10.1126/science.291.5501.109>.
- Boswell, S.M., Toucanne, S., Pitel-Roudaut, M., Creyts, T.T., Eynaud, F., Bayon, G., 2019. Enhanced surface melting of the Fennoscandian Ice Sheet during periods of North Atlantic cooling. *Geology* 47, 664–668. <https://doi.org/10.1130/G46370.1>.
- Boyle, E.A., Lea, D.W., 1989. Cd and Ba in planktonic foraminifera from the eastern Mediterranean: evidence for river outflow and enriched nutrients during sapropel formation. *Trans. Am. Geophys. Union* 70, 1134.
- Brand, L.E., 1994. Physiological ecology of marine coccolithophores. *Coccolithophores* 39–50.
- Broecker, W.S., 1998. Paleocene circulation during the last Deglaciation: a bipolar seesaw? *Paleoceanography* 13, 119–121. <https://doi.org/10.1029/97PA03707>.
- Cachao, M., Moita, M.T., 2000. Coccolithus pelagicus, a productivity proxy related to moderate fronts off Western Iberia. *Mar. Micropaleontol.* 39, 131–155. [https://doi.org/10.1016/S0377-8398\(00\)00018-9](https://doi.org/10.1016/S0377-8398(00)00018-9).
- Calvert, S.E., 1983. Geochemistry of Pleistocene sapropels and associated sediments from the Eastern Mediterranean. *Oceanol. Acta* 6, 255–267.
- Calvert, S.E., Fontugne, M.R., 2001. On the late Pleistocene-Holocene sapropel record of climatic and oceanographic variability in the eastern Mediterranean. *Paleoceanography* 16, 78–94. <https://doi.org/10.1029/1999PA000488>.
- Calvert, S.E., Pedersen, T.F., 1993. Geochemistry of recent oxic and anoxic marine sediments: implications for the geological record. *Mar. Geol.* 113, 67–88. [https://doi.org/10.1016/0025-3227\(93\)90150-T](https://doi.org/10.1016/0025-3227(93)90150-T).
- Calvert, S.E., Nielsen, B., Fontugne, M.R., 1992. Evidence from nitrogen isotope ratios for enhanced productivity during formation of eastern Mediterranean sapropels. *Nature* 359, 223–225. <https://doi.org/10.1038/359223a0>.
- Capotondi, L., Vigliotti, L., Bergami, C., Sangiorgi, F., 2011. In: *Dipartimento Terra e Ambiente—CNR (Ed.), The Dark Side of the Mediterranean Geological Record: the sapropel layers and a case study from the Ionian Sea. Marine Research at CNR. CNR, Roma*, pp. 658–669.
- Casford, J.S.L., Rohling, E.J., Abu-Zied, R.H., Fontanier, C., Jorissen, F.J., Leng, M.J., Schmiedl, G., Thomson, J., 2003. A dynamic concept for eastern Mediterranean circulation and oxygenation during sapropel formation. *Palaeogeogr. Palaeoclimatol. Palaeoecol.* 190, 103–119.
- Castradori, D., 1993. Calcareous nannofossils and the origin of eastern Mediterranean sapropels. *Paleoceanography* 8, 459–471. <https://doi.org/10.1029/93PA00756>.
- Cheng, H., Edwards, R.L., Sinha, A., Spötl, C., Yi, L., Chen, S., Kelly, M., Kathayat, G., Wang, X., Li, X., 2016. The Asian monsoon over the past 640,000 years and ice age terminations. *Nature* 534, 640–646. <https://doi.org/10.1038/nature18591>.
- Cita, M.B., 1982. Nature and Origin of late Neogene Mediterranean Sapropels. *Nature and Origin of Cretaceous Carbon-Rich Facies*, pp. 165–196.
- Cita, M.B., Vergnaud-Grazzini, C., Robert, C., Chamley, H., Ciaranfi, N., d'Onofrio, S., 1977. Paleoclimatic record of a long deep sea core from the eastern Mediterranean. *Quat. Res.* 8, 205–235. [https://doi.org/10.1016/0033-5894\(77\)90046-1](https://doi.org/10.1016/0033-5894(77)90046-1).
- Cita, M.B., Beghi, C., Camerlenghi, A., Kastens, K.A., McCoy, F.W., Nassetto, A., Parisi, E., Scolari, F., Tomadin, L., 1984. Turbidites and megaturbidites from the Herodotus abyssal plain (eastern Mediterranean) unrelated to seismic events. *Mar. Geol.* 55, 79–101. [https://doi.org/10.1016/0025-3227\(84\)90134-8](https://doi.org/10.1016/0025-3227(84)90134-8).
- Colleoni, F., Liakka, J., 2020. Transient Simulations of the Eurasian Ice Sheet during the Saalian Glacial Cycle. *SVENSK KÄRNBRÄNSLEHANTERING AB, Stockholm*. SKB TR-19-17. <https://www.skb.com/publication/2494735>.
- Colleoni, F., Masina, S., Negri, A., Marzocchi, A., 2012. Plio-Pleistocene high-low latitude climate interplay: a Mediterranean point of view. *Earth Planet. Sci. Lett.* 319, 35–44.
- Columbu, A., Sauro, F., Lundberg, J., Drysdale, R., De Waele, J., 2018. Palaeoenvironmental changes recorded by speleothems of the southern Alps (Piani Eterni, Belluno, Italy) during four interglacial to glacial climate transitions. *Quat. Sci. Rev.* 197, 319–335. <https://doi.org/10.1016/j.quascirev.2018.08.006>.
- Corselli, C., Principato, M.S., Maffioli, P., Crudeli, D., 2002. Changes in planktonic assemblages during sapropel S5 deposition: evidence from Urania Basin area, eastern Mediterranean. *Paleoceanography* 17. <https://doi.org/10.1029/2000PA000536>.
- Cros, L., Kleijne, A., Zeltner, A., Billard, C., Young, J.R., 2000. New examples of holococcolith-heterococcolith combination coccospheres and their implications for coccolithophorid biology. *Mar. Micropaleontol.* 39, 1–34. [https://doi.org/10.1016/S0377-8398\(00\)00010-4](https://doi.org/10.1016/S0377-8398(00)00010-4).
- Dale, B., 2009. Eutrophication signals in the sedimentary record of dinoflagellate cysts in coastal waters. *J. Sea Res.* 61, 103–113. <https://doi.org/10.1016/j.seares.2008.06.007>.
- de Abreu, L., Shackleton, N.J., Schönfeld, J., Hall, M., Chapman, M., 2003. Millennial-scale oceanic climate variability off the Western Iberian margin during the last two glacial periods. *Mar. Geol.* 196, 1–20. [https://doi.org/10.1016/S0025-3227\(03\)00046-X](https://doi.org/10.1016/S0025-3227(03)00046-X).
- De Lange, G.J., Ten Haven, H.L., 1983. Recent sapropel formation in the eastern Mediterranean. *Nature* 305, 797–798.
- De Lange, G.J., Thomson, J., Reitz, A., Slomp, C.P., Speranza Principato, M., Erba, E., Corselli, C., 2008. Synchronous basin-wide formation and redox-controlled preservation of a Mediterranean sapropel. *Nat. Geosci.* 1, 606–610. <https://doi.org/10.1038/ngeo283>.
- Dimiza, M.D., Triantaphyllou, M.V., Malinverno, E., 2014. New evidence for the ecology of *Helicospaera carteri* in polluted coastal environments (Elefsis Bay, Saronikos Gulf, Greece). *J. Nannoplankton Res.* 34, 37–43.
- Ding, Z.L., Ren, J.Z., Yang, S.L., Liu, T.S., 1999. Climate instability during the penultimate glaciation: evidence from two high-resolution loess records, China. *J. Geophys. Res.* 104, 20123–20132. <https://doi.org/10.1029/1999JB900183>.
- Dirksen, J.P., Meijer, P., 2020. The mechanism of sapropel formation in the Mediterranean Sea: insight from long-duration box model experiments. *Clim. Past* 16, 933–952. <https://doi.org/10.5194/cp-16-933-2020>, 2020.
- Donders, T., Panagiotopoulos, K., Koutsodendris, A., Bertini, A., Mercuri, A.M., Masi, A., Combourieu-Nebout, N., Joannin, S., Kouli, K., Kousis, I., Peyron, O., Torri, P., Florenzano, A., Francke, A., Wagner, B., Sadori, L., 2021. 1.36 million years of Mediterranean forest refugium dynamics in response to glacial-interglacial cycle

- strength. *Proc. Natl. Acad. Sci. USA* 118, e2026111118. <https://doi.org/10.1073/pnas.2026111118>.
- Ehlers, J., Gibbard, P.L., Hughes, P.D., 2018. Quaternary glaciations and chronology. In: *Past Glacial Environments*. Elsevier, pp. 77–101. <https://doi.org/10.1016/B978-0-08-100524-8.00003-8>.
- Emeis, K.C., Party, S.S., 1996. Paleooceanography and sapropel introduction. In: Emeis, K.-C., Robertson, A.H.F., Richter, C., et al. (Eds.), *Proc. ODP, Init. Repts.*, pp. 21–28.
- Emeis, K.-C., Schulz, H., Struck, U., Rossignol-Strick, M., Erlenkeuser, H., Howell, M.W., Kroon, D., Mackensen, A., Ishizuka, S., Oba, T., Sakamoto, T., Koizumi, I., 2003. Eastern Mediterranean surface water temperatures and  $\delta^{18}\text{O}$  composition during deposition of sapropels in the late Quaternary. *Paleoceanography* 18. <https://doi.org/10.1029/2000PA000617>.
- Emiliani, C., 1955. Pleistocene Temperatures. *J. Geol.* 63, 538–578. <https://doi.org/10.1086/626295>.
- Eynaud, F., Zaragosi, S., Scourse, J.D., Mojtahid, M., Bourillet, J.F., Hall, I.R., Penaud, A., Locascio, M., Reijonen, A., 2007. Deglacial laminated facies on the NW European continental margin: the hydrographic significance of British-Irish Ice Sheet deglaciation and Fleuve Manche paleoriver discharges. *Geochim. Geophys. Geosyst.* 8. <https://doi.org/10.1029/2006GC001496>.
- Filippidi, A., De Lange, G.J., 2019. Eastern Mediterranean Deep Water Formation during Sapropel S1: a Reconstruction using Geochemical Records along a Bathymetric Transect in the Adriatic Outflow Region. *Paleoceanog. Paleoclimatol.* 34, 409–429. <https://doi.org/10.1029/2018PA003459>.
- Findlay, C.S., Giraudeau, J., 2000. Extant calcareous nannoplankton in the Australian Sector of the Southern Ocean (austral summers 1994 and 1995). *Mar. Micropaleontol.* 40, 417–439. [https://doi.org/10.1016/S0377-8398\(00\)00046-3](https://doi.org/10.1016/S0377-8398(00)00046-3).
- Findlay, C.S., Giraudeau, J., 2002. Movement of oceanic fronts south of Australia during the last 10 ka: interpretation of calcareous nannoplankton in surface sediments from the Southern Ocean. *Mar. Micropaleontol.* 46, 431–444. [https://doi.org/10.1016/S0377-8398\(02\)00084-1](https://doi.org/10.1016/S0377-8398(02)00084-1).
- Flores, J.A., Sierro, F.J., 1997. Revised technique for calculation of calcareous nannofossil accumulation rates. *Micropaleontology* 321–324. <https://doi.org/10.2307/1485832>.
- Fontugne, M.R., Calvert, S.E., 1992. Late Pleistocene Variability of the Carbon Isotopic Composition of Organic Matter in the Eastern Mediterranean: Monitor of changes in Carbon sources and Atmospheric  $\text{CO}_2$  Concentrations. *Paleoceanography* 7, 1–20. <https://doi.org/10.1029/91PA02674>.
- Gartner, S., Chow, J., Stanton Jr., R.J., 1987. Late Neogene paleoceanography of the eastern Caribbean, the Gulf of Mexico, and the eastern equatorial Pacific. *Mar. Micropaleontol.* 12, 255–304. [https://doi.org/10.1016/0377-8398\(87\)90024-7](https://doi.org/10.1016/0377-8398(87)90024-7).
- Genty, D., Blamart, D., Ouahdi, R., Gilmour, M., Baker, A., Jouzel, J., Van-Exter, S., 2003. Precise dating of Dansgaard-Oeschger climate oscillations in western Europe from stalagmite data. *Nature* 421, 833–837. <https://doi.org/10.1038/nature01391>.
- Giraudeau, J., 1992. Distribution of recent nannofossils beneath the Benguela system: southwest African continental margin. *Mar. Geol.* 108, 219–237. [https://doi.org/10.1016/0025-3227\(92\)90174-G](https://doi.org/10.1016/0025-3227(92)90174-G).
- Grant, K.M., Rohling, E.J., Bar-Matthews, M., Ayala, A., Medina-Elizalde, M., Ramsey, C.B., Satow, C., Roberts, A.P., 2012. Rapid coupling between ice volume and polar temperature over the past 150,000 years. *Nature* 491, 744–747. <https://doi.org/10.1038/nature11593>.
- Grant, K.M., Rohling, E.J., Ramsey, C.B., Cheng, H., Edwards, R.L., Florindo, F., Heslop, D., Marra, F., Roberts, A.P., Tamisieva, M.E., 2014. Sea-level variability over five glacial cycles. *Nat. Commun.* 5, 5076. <https://doi.org/10.1038/ncomms6076>.
- Grant, K.M., Grimm, R., Mikolajewicz, U., Marino, G., Ziegler, M., Rohling, E.J., 2016. The timing of Mediterranean sapropel deposition relative to insolation, sea-level and African monsoon changes. *Quat. Sci. Rev.* 140, 125–141. <https://doi.org/10.1016/j.quascirev.2016.03.026>.
- Grant, K.M., Rohling, E.J., Westerhold, T., Zabel, M., Heslop, D., Konijnendijk, T., Lourens, L., 2017. A 3 million year index for North African humidity/aridity and the implication of potential pan-African Humid periods. *Quat. Sci. Rev.* 171, 100–118. <https://doi.org/10.1016/j.quascirev.2017.07.005>.
- Grant, K.M., Amarathunga, U., Amies, J.D., Hu, P., Qian, Y., Penny, T., Rodríguez-Sanz, L., Zhao, X., Heslop, D., Liebrand, D., 2022. Organic carbon burial in Mediterranean sapropels intensified during Green Sahara periods since 3.2 Myr ago. *Commun. Earth Environ.* 3, 11. <https://doi.org/10.1038/s43247-021-00339-9>.
- Grelaud, M., Marino, G., Ziveri, P., Rohling, E.J., 2012. Abrupt shoaling of the nutricline in response to massive freshwater flooding at the onset of the last interglacial sapropel event. *Paleoceanography* 27. <https://doi.org/10.1029/2012PA002288>.
- Grimm, R., Maier-Reimer, E., Mikolajewicz, U., Schmiedl, G., Müller-Navarra, K., Adloff, F., Grant, K.M., Ziegler, M., Lourens, L.J., Emeis, K.-C., 2015. Late glacial initiation of Holocene eastern Mediterranean sapropel formation. *Nat. Commun.* 6, 7099. <https://doi.org/10.1038/ncomms8099>.
- Halim, Y., Guergues, S.K., Saleh, H.H., 1967. Hydrographic Conditions and Plankton in the South East Mediterranean during the last Normal Nile Flood (1964). *Int. Rev. Hydrobiol.* 52, 401–425. <https://doi.org/10.1002/iroh.19670520305>.
- Hayes, A., Kucera, M., Kallel, N., Saffi, L., Rohling, E.J., 2005. Glacial Mediterranean Sea surface temperatures based on planktonic foraminiferal assemblages. *Quat. Sci. Rev.* 24, 999–1016. <https://doi.org/10.1016/j.quascirev.2004.02.018>.
- van Helmond, N.A., Sluijs, A., Sinnighe Damsté, J.S., Reichert, G.-J., Voigt, S., Erbacher, J., Pross, J., Brinkhuis, H., 2015. Freshwater discharge controlled deposition of Cenomanian–Turonian black shales on the NW European epicontinental shelf (Wunstorf, northern Germany). *Clim. Past* 11, 495–508. <https://doi.org/10.5194/cp-11-495-2015>.
- Heslop, D., Amarathunga, U., Rohling, E.J., 2023. Estimating Plio-Pleistocene North African Monsoon Runoff into the Mediterranean Sea and Temperature Impacts. *Paleoceanog. Paleoclimatol.* 38. <https://doi.org/10.1029/2023PA004677>.
- Hodell, D., Lourens, L., Crowhurst, S., Konijnendijk, T., Tjallingii, R., Jiménez-Espejo, F., Skinner, L., Tzedakis, P.C., Members, T.S.S.P., Abrantes, F., 2015. A reference time scale for Site U1385 (Shackleton Site) on the SW Iberian margin. *Glob. Planet. Chang.* 133, 49–64.
- Hodell, D., Crowhurst, S., Lourens, L., Margari, V., Nicolson, J., Rolfé, J.E., Skinner, L.C., Thomas, N., Tzedakis, P.C., Mleneck-Vautravers, M.J., 2022. A 1.5-million-year record of orbital and millennial climate variability in the North Atlantic. *Clim. Past Discuss.* 2022, 1–58.
- Hutson, W.H., 1980. The Agulhas current during the late Pleistocene: analysis of modern faunal analogs. *Science* 207, 64–66. <https://doi.org/10.1126/science.207.4426.64>.
- Incarbona, A., Ziveri, P., Sabatino, N., Manta, D.S., Sprovieri, M., 2011. Conflicting coccolithophore and geochemical evidence for productivity levels in the Eastern Mediterranean sapropel S1. *Mar. Micropaleontol.* 81, 131–143. <https://doi.org/10.1016/j.marmicro.2011.09.003>.
- Incarbona, A., Marino, G., Di Stefano, E., Grelaud, M., Pelosi, N., Rodríguez-Sanz, L., Rohling, E.J., 2022. Middle-late Pleistocene eastern Mediterranean nutricline depth and coccolith preservation linked to Monsoon activity and Atlantic meridional overturning circulation. *Glob. Planet. Chang.* 217, 103946.
- Jorissen, F.J., 1999. Benthic foraminiferal successions across late Quaternary Mediterranean sapropels. *Mar. Geol.* 153, 91–101. [https://doi.org/10.1016/S0025-3227\(98\)00088-7](https://doi.org/10.1016/S0025-3227(98)00088-7).
- Jorissen, F.J., Asioli, A., Borsetti, A.M., Capotondi, L., De Visser, J.P., Hilgen, F.J., Rohling, E.J., Van der Borg, K., Grazzini, C.V., Zachariasse, W.J., 1993. Late quaternary Central Mediterranean biochronology. *Mar. Micropaleontol.* 21, 169–189. [https://doi.org/10.1016/0377-8398\(93\)90014-0](https://doi.org/10.1016/0377-8398(93)90014-0).
- Kallel, N., Paterne, M., Duplessy, J.C., Vergnaudgrazini, C., Pujol, C., Labeyrie, L., Arnold, M., Fontugne, M., Pierre, C., 1997. Enhanced rainfall in the Mediterranean region during the last sapropel event. *Oceanol. Acta* 20, 697–712.
- Kallel, N., Duplessy, J.-C., Labeyrie, L., Fontugne, M., Paterne, M., Montacer, M., 2000. Mediterranean pluvial periods and sapropel formation over the last 200 000 years. *Palaeogeogr. Palaeoclimatol. Palaeoecol.* 157, 45–58. [https://doi.org/10.1016/S0031-0182\(99\)00149-2](https://doi.org/10.1016/S0031-0182(99)00149-2).
- Keller, J., Ryan, W.B.F., Ninkovich, D., Altherr, R., 1978. Explosive volcanic activity in the Mediterranean over the past 200,000 yr as recorded in deep-sea sediments. *Geol. Soc. Am. Bull.* 89, 591–604. [https://doi.org/10.1130/0016-7606\(1978\)89<591:EVAITM>2.0.CO;2](https://doi.org/10.1130/0016-7606(1978)89<591:EVAITM>2.0.CO;2).
- Kidd, R.B., 1978. Stratigraphy of eastern Mediterranean sapropel sequences recovered during Leg 42A and their paleoenvironmental significance. *Initial Rep. Deep Sea Drill. Proj.* 42, 421–443.
- Konijnendijk, T.Y.M., Ziegler, M., Lourens, L.J., 2014. Chronological constraints on Pleistocene sapropel depositions from high-resolution geochemical records of ODP Sites 967 and 968. *News. Stratigr.* 47, 263–282. <https://doi.org/10.1127/0078-0421/2014/0047>.
- Kraml, M., 1997. *Laser-40 Ar, 39 Ar-Datierungen an distalen marinen Tephren des jung-quartären mediterranen Vulkanismus (Ionisches Meer, METEOR-Fahrt 25/4)* (PhD Thesis). Verlag nicht ermittelbar.
- Kullenberg, B., 1952. On the Salinity of the Water Contained in Marine Sediments. *Elanders boktr.*
- Larrasaña, J.C., Roberts, A.P., Rohling, E.J., 2013. Dynamics of green Sahara periods and their role in hominin evolution. *PLoS One* 8, e76514. <https://doi.org/10.1371/journal.pone.0076514>.
- Limoges, A., Londeix, L., de Vernal, A., 2013. Organic-walled dinoflagellate cyst distribution in the Gulf of Mexico. *Mar. Micropaleontol.* 102, 51–68. <https://doi.org/10.1016/j.marmicro.2013.06.002>.
- Mangini, A., Schlosser, P., 1986. The formation of eastern Mediterranean sapropels. *Mar. Geol.* 72, 115–124. [https://doi.org/10.1016/0025-3227\(86\)90102-7](https://doi.org/10.1016/0025-3227(86)90102-7).
- Margari, V., Skinner, L.C., Tzedakis, P.C., Ganopolski, A., Vautravers, M., Shackleton, N. J., 2010. The nature of millennial-scale climate variability during the past two glacial periods. *Nat. Geosci.* 3, 127–131. <https://doi.org/10.1038/ngeo740>.
- Margari, V., Skinner, L.C., Hodell, D.A., Martrat, B., Toucanne, S., Grimalt, J.O., Gibbard, P.L., Lunkka, J.P., Tzedakis, P.C., 2014. Land-ocean changes on orbital and millennial time scales and the penultimate glaciation. *Geology* 42, 183–186.
- Marino, G., Zahn, R., Ziegler, M., Purcell, C., Knorr, G., Hall, I.R., Ziveri, P., Elderfield, H., 2013. Agulhas salt-leakage oscillations during abrupt climate changes of the late Pleistocene. *Paleoceanography* 28, 599–606. <https://doi.org/10.1002/palo.20038>.
- Marino, G., Rohling, E.J., Rodríguez-Sanz, L., Grant, K.M., Heslop, D., Roberts, A.P., Stanford, J.D., Yu, J., 2015. Bipolar seesaw control on last interglacial sea level. *Nature* 522, 197–201. <https://doi.org/10.1038/nature14499>.
- Martrat, B., Grimalt, J.O., Lopez-Martinez, C., Cacho, I., Sierro, F.J., Flores, J.A., Zahn, R., Canals, M., Curtis, J.H., Hodell, D.A., 2004. Abrupt temperature changes in the Western Mediterranean over the past 250,000 years. *Science* 306, 1762–1765. <https://doi.org/10.1126/science.1101706>.
- Martrat, B., Grimalt, J.O., Shackleton, N.J., De Abreu, L., Hutterli, M.A., Stocker, T.F., 2007. Four climate Cycles of Recurring deep and Surface Water Destabilizations on the Iberian margin. *Science* 317, 502–507. <https://doi.org/10.1126/science.1139994>.
- McIntyre, A., Bé, A.W., 1967. Modern coccolithophoridae of the Atlantic Ocean—I. Placoliths and cyrtoliths. In: *Deep Sea Research and Oceanographic Abstracts*. Elsevier, pp. 561–597. [https://doi.org/10.1016/0011-7471\(67\)90065-4](https://doi.org/10.1016/0011-7471(67)90065-4).
- Mercone, D., Thomson, J., Abu-Zied, R.H., Croudace, I.W., Rohling, E.J., 2001. High-resolution geochemical and micropaleontological profiling of the most recent

- eastern Mediterranean sapropel. *Mar. Geol.* 177, 25–44. [https://doi.org/10.1016/S0025-3227\(01\)00122-0](https://doi.org/10.1016/S0025-3227(01)00122-0).
- Murat, A., Got, H., 1987. Middle and late Quaternary depositional sequences and cycles in the eastern Mediterranean. *Sedimentology* 34, 885–899. <https://doi.org/10.1111/j.1365-3091.1987.tb00810.x>.
- Myers, P.G., Haines, K., Rohling, E.J., 1998. Modeling the paleocirculation of the Mediterranean: the last Glacial Maximum and the Holocene with emphasis on the formation of sapropel S<sub>1</sub>. *Paleoceanography* 13, 586–606. <https://doi.org/10.1029/98PA02736>.
- Narcisi, B., Vezzoli, L., 1999. Quaternary stratigraphy of distal tephra layers in the Mediterranean—an overview. *Glob. Planet. Chang.* 21, 31–50. [https://doi.org/10.1016/S0921-8181\(99\)00006-5](https://doi.org/10.1016/S0921-8181(99)00006-5).
- Negri, A., Capotondi, L., Keller, J., 1999. Calcareous nannofossils, planktonic foraminifera and oxygen isotopes in the late Quaternary sapropels of the Ionian Sea. *Mar. Geol.* 157, 89–103. [https://doi.org/10.1016/S0025-3227\(98\)00135-2](https://doi.org/10.1016/S0025-3227(98)00135-2).
- Negri, A., Morigi, C., Giunta, S., 2003. Are productivity and stratification important to sapropel deposition? Microfossil evidence from late Pliocene insolation cycle 180 at Vrica, Calabria. *Palaeogeogr. Palaeoclimatol. Palaeoecol.* 190, 243–255. [https://doi.org/10.1016/S0031-0182\(02\)00608-9](https://doi.org/10.1016/S0031-0182(02)00608-9).
- Nehme, C., Verheyden, S., Breitenbach, S.F., Gillikin, D.P., Verheyden, A., Cheng, H., Edwards, R.L., Hellstrom, J., Noble, S.R., Farrant, A.R., 2018. Climate dynamics during the penultimate glacial period recorded in a speleothem from Kanaan Cave, Lebanon (central Levant). *Quat. Res.* 90, 10–25. <https://doi.org/10.1017/qua.2018.18>.
- Nijenhuis, I.A., de Lange, G.J., 2000. Geochemical constraints on Pliocene sapropel formation in the eastern Mediterranean. *Mar. Geol.* 163, 41–63. [https://doi.org/10.1016/S0025-3227\(99\)00093-6](https://doi.org/10.1016/S0025-3227(99)00093-6).
- Obrochta, S.P., Crowley, T.J., Channell, J.E., Hodell, D.A., Baker, P.A., Seki, A., Yokoyama, Y., 2014. Climate variability and ice-sheet dynamics during the last three glaciations. *Earth Planet. Sci. Lett.* 406, 198–212. <https://doi.org/10.1016/j.epsl.2014.09.004>.
- Okada, H., McIntyre, A., 1979. Seasonal distribution of modern coccolithophores in the western North Atlantic Ocean. *Mar. Biol.* 54, 319–328. <https://doi.org/10.1007/BF00395438>.
- Olausson, E., 1961. Studies in deep-sea cores. Reports Swedish Deep-Sea Exped. 1947–1948 (8), 337–391.
- Osborne, A.H., Vance, D., Rohling, E.J., Barton, N., Rogerson, M., Fello, N., 2008. A humid corridor across the Sahara for the migration of early modern humans out of Africa 120,000 years ago. *Proc. Natl. Acad. Sci. USA* 105, 16444–16447. <https://doi.org/10.1073/pnas.0804472105>.
- Parisi, E., Cita, M.B., 1982. Late Quaternary paleoceanographic changes recorded by deep-sea benthos in the western Mediterranean ridge. *Geogr. Fis. Din. Quat.* 5, 102–114.
- Parisi, E., Erba, E., Cita, M.B., 1987. Stratigraphy and sedimentation in the anoxic Bannock Basin (Eastern Mediterranean). *Mar. Geol.* 75, 93–117. [https://doi.org/10.1016/0025-3227\(87\)90098-3](https://doi.org/10.1016/0025-3227(87)90098-3).
- Patterson, R.T., Fishbein, E., 1989. Re-examination of the statistical methods used to determine the number of point counts needed for micropaleontological quantitative research. *J. Paleontol.* 63, 245–248.
- Pedro, J.B., Jochum, M., Buizert, C., He, F., Barker, S., Rasmussen, S.O., 2018. Beyond the bipolar seesaw: toward a process understanding of interhemispheric coupling. *Quat. Sci. Rev.* 192, 27–46.
- Peeters, F., Ivanova, E., Conan, S., Brummer, G.-J., Ganssen, G., Troelstra, S., van Hinte, J., 1999. A size analysis of planktic foraminifera from the Arabian Sea. *Mar. Micropaleontol.* 36, 31–63.
- Piva, A., Asioli, A., Andersen, N., Grimalt, J.O., Schneider, R.R., Trincardi, F., 2008. Climatic cycles as expressed in sediments of the PROMESS1 borehole PRAD1-2, central Adriatic, for the last 370 ka: 2. Paleoenvironmental evolution. *Geochem. Geophys. Geosyst.* 9 <https://doi.org/10.1029/2007GC001785>, 2007GC001785.
- Radi, T., de Vernal, A., 2008. Dinocysts as proxy of primary productivity in mid-high latitudes of the Northern Hemisphere. *Mar. Micropaleontol.* 68, 84–114. <https://doi.org/10.1016/j.marmicro.2008.01.012>.
- Raffi, I., Rio, D., 1981. *Coccolithus pelagicus* (Wallich): a paleotemperature indicator in the late Pliocene Mediterranean deep sea record. In: *Consiglio Nazionale Delle Ricerche. International Conference*, pp. 187–190.
- Railsback, L.B., Gibbard, P.L., Head, M.J., Voarintsoa, N.R.G., Toucanne, S., 2015. An optimized scheme of lettered marine isotope substages for the last 1.0 million years, and the climatostratigraphic nature of isotope stages and substages. *Quat. Sci. Rev.* 111, 94–106. <https://doi.org/10.1016/j.quascirev.2015.01.012>.
- Reed, D.C., Slomp, C.P., de Lange, G.J., 2011. A quantitative reconstruction of organic matter and nutrient diagenesis in Mediterranean Sea sediments over the Holocene. *Geochim. Cosmochim. Acta* 75, 5540–5558. <https://doi.org/10.1016/j.gca.2011.07.002>.
- Regattieri, E., Zanchetta, G., Drysdale, R.N., Isola, I., Hellstrom, J.C., Roncioni, A., 2014. A continuous stable isotope record from the penultimate glacial maximum to the last Interglacial (159–121 ka) from Tana Che Urla Cave (Apuan Alps, Central Italy). *Quat. Res.* 82, 450–461. <https://doi.org/10.1016/j.yqres.2014.05.005>.
- Regattieri, E., Querci, S., Zanchetta, G., Zanella, E., Isola, I., Drysdale, R.N., Hellstrom, J. C., Magri, F., 2021. Interstadial conditions over the Southern Alps during the early penultimate glacial (MIS 6): a multiproxy record from Rio Martino Cave (Italy). *Quat. Sci. Rev.* 257, 106856 <https://doi.org/10.1016/j.quascirev.2021.106856>.
- Reille, M., 1992. New pollen-analytical researches in Corsica: the problem of *Quercus ilex* L. and *Erica arborea* L., the origin of *Pinus halepensis* Miller forests. *New Phytol.* 122, 359–378. <https://doi.org/10.1111/j.1469-8137.1992.tb04241.x>.
- Reitz, A., Thomson, J., De Lange, G.J., Hensen, C., 2006. Source and development of large manganese enrichments above eastern Mediterranean sapropel S1. *Paleoceanography* 21. <https://doi.org/10.1029/2005PA001169>, 2005PA001169.
- Rodríguez-Sanz, L., Bernasconi, S.M., Marino, G., Heslop, D., Mueller, I.A., Fernandez, A., Grant, K.M., Rohling, E.J., 2017. Penultimate deglacial warming across the Mediterranean Sea revealed by clumped isotopes in foraminifera. *Sci. Rep.* 7, 16572. <https://doi.org/10.1038/s41598-017-16528-6>.
- Rohling, E.J., 1994. Review and new aspects concerning the formation of eastern Mediterranean sapropels. *Mar. Geol.* 122, 1–28. [https://doi.org/10.1016/0025-3227\(94\)90202-X](https://doi.org/10.1016/0025-3227(94)90202-X).
- Rohling, E.J., 1999. Environmental control on Mediterranean salinity and  $\delta^{18}\text{O}$ . *Paleoceanography* 14, 706–715. <https://doi.org/10.1029/1999PA000042>.
- Rohling, E.J., Gieskes, W.W.C., 1989. Late Quaternary changes in Mediterranean intermediate water density and formation rate. *Paleoceanography* 4, 531–545. <https://doi.org/10.1029/PA004i005p00531>.
- Rohling, E.J., Hilgen, F.J., 1991. The eastern Mediterranean climate at times of sapropel formation: a review. *Geol. Mijnb.* 70, 253–264.
- Rohling, E.J., Pälike, H., 2005. Centennial-scale climate cooling with a sudden cold event around 8,200 years ago. *nature* 434, 975–979. <https://doi.org/10.1038/nature03421>.
- Rohling, E.J., Jorissen, F.J., Grazzini, C.V., Zachariasse, W.J., 1993. Northern Levantine and Adriatic Quaternary planktic foraminifera: Reconstruction of paleoenvironmental gradients. *Mar. Micropaleontol.* 21, 191–218.
- Rohling, E.J., Jorissen, F.J., De Stigter, H.C., 1997. 200 year interruption of Holocene sapropel formation in the Adriatic Sea. *J. Micropaleontol.* 16, 97–108.
- Rohling, E.J., Cane, T.R., Cooke, S., Sprovieri, M., Bouloubassi, I., Emeis, K.C., Schiebel, R., Kroon, D., Jorissen, F.J., Llorca, A., 2002. African monsoon variability during the previous interglacial maximum. *Earth Planet. Sci. Lett.* 202, 61–75.
- Rohling, E.J., Sprovieri, M., Cane, T., Casford, J.S., Cooke, S., Bouloubassi, I., Emeis, K. C., Schiebel, R., Rogerson, M., Hayes, A., 2004. Reconstructing past planktic foraminiferal habitats using stable isotope data: a case history for Mediterranean sapropel S5. *Mar. Micropaleontol.* 50, 89–123. [https://doi.org/10.1016/S0307-7839\(03\)00068-9](https://doi.org/10.1016/S0307-7839(03)00068-9).
- Rohling, E.J., Abu-Zied, R., Casford, J.S.L., Hayes, A., Hoogakker, B.A.A., 2009. The marine environment: present and past. *Phys. Geogr. Mediterran.* 8, 33.
- Rohling, E.J., Foster, G.L., Grant, K.M., Marino, G., Roberts, A.P., Tamsiea, M.E., Williams, F., 2014. Sea-level and deep-sea-temperature variability over the past 5.3 million years. *Nature* 508, 477–482.
- Rohling, E.J., Marino, G., Grant, K.M., 2015. Mediterranean climate and oceanography, and the periodic development of anoxic events (sapropels). *Earth Sci. Rev.* 143, 62–97.
- Rohling, E.J., Hibbert, F.D., Williams, F.H., Grant, K.M., Marino, G., Foster, G.L., Hennekam, R., de Lange, G.J., Roberts, A.P., Yu, J., Webster, J.M., Yokoyama, Y., 2017. Differences between the last two glacial maxima and implications for ice-sheet,  $\delta^{18}\text{O}$ , and sea-level reconstructions. *Quat. Sci. Rev.* 176, 1–28. <https://doi.org/10.1016/j.quascirev.2017.09.009>.
- Rossignol-Strick, M., 1983. African monsoons, an immediate climate response to orbital insolation. *Nature* 304, 46–49. <https://doi.org/10.1038/304046a0>.
- Rossignol-Strick, M., 1985. Mediterranean Quaternary sapropels, an immediate response of the African monsoon to variation of insolation. *Paleoceanogr. Palaeoecol.* 49, 237–263. [https://doi.org/10.1016/0031-0182\(85\)90056-2](https://doi.org/10.1016/0031-0182(85)90056-2).
- Rossignol-Strick, M., Paterne, M., 1999. A synthetic pollen record of the eastern Mediterranean sapropels of the last 1 Ma: implications for the time-scale and formation of sapropels. *Mar. Geol.* 153, 221–237. [https://doi.org/10.1016/S0025-3227\(98\)00080-2](https://doi.org/10.1016/S0025-3227(98)00080-2).
- Rossignol-Strick, M., Nesteroff, W., Olive, P., Vergnaud-Grazzini, C., 1982. After the deluge: Mediterranean stagnation and sapropel formation. *Nature* 295, 105–110. <https://doi.org/10.1038/295105a0>.
- Roucoux, K.H., Tzedakis, P.C., Lawson, I.T., Margari, V., 2011. Vegetation history of the penultimate glacial period (Marine isotope stage 6) at Ioannina, north-West Greece. *J. Quat. Sci.* 26, 616–626. <https://doi.org/10.1002/jqs.1483>.
- Rousseau, D.-D., Antoine, P., Boers, N., Lagroix, F., Ghil, M., Lomax, J., Fuchs, M., Debret, M., Hatté, C., Moine, O., 2020. Dansgaard-Oeschger-like events of the penultimate climate cycle: the loess point of view. *Clim. Past* 16, 713–727. <https://doi.org/10.5194/cp-16-713-2020>.
- Ryan, W.B., Cita, M.B., 1977. Ignorance concerning episodes of ocean-wide stagnation. *Mar. Geol.* 23, 197–215.
- Ryan, W.B.F., 1972. Stratigraphy of late Quaternary sediments in the eastern Mediterranean. *Mediterranean Sea* 765.
- Sabbatini, A., Bonatto, S., Bianchelli, S., Pusceddu, A., Danovaro, R., Negri, A., 2012. Foraminiferal assemblages and trophic state in coastal sediments of the Adriatic Sea. *J. Mar. Syst.* 105, 163–174. <https://doi.org/10.1016/j.jmarsys.2012.07.009>.
- Sangiorgi, F., Donders, T.H., 2004. Reconstructing 150 years of eutrophication in the North-Western Adriatic Sea (Italy) using dinoflagellate cysts, pollen and spores. *Estuar. Coast. Shelf Sci.* 60, 69–79. <https://doi.org/10.1016/j.ecss.2003.12.001>.
- Sangiorgi, F., Capotondi, L., Brinkhuis, H., 2002. A centennial scale organic-walled dinoflagellate cyst record of the last deglaciation in the South Adriatic Sea (Central Mediterranean). *Palaeogeogr. Palaeoclimatol. Palaeoecol.* 186, 199–216.
- Sangiorgi, F., Capotondi, L., Combourieu Nebout, N., Vigliotti, L., Brinkhuis, H., Giunta, S., Lotter, A.F., Morigi, C., Negri, A., Reichart, G., 2003. Holocene seasonal sea-surface temperature variations in the southern Adriatic Sea inferred from a multiproxy approach. *J. Quat. Sci.* 18, 723–732. <https://doi.org/10.1002/jqs.782>.
- Schiebel, R., Hemleben, C., 2017. Planktic Foraminifera in the Modern Ocean. Springer Berlin Heidelberg, Berlin, Heidelberg. <https://doi.org/10.1007/978-3-662-50297-6>.



- Schmiedl, G., Hemleben, C., Keller, J., Segl, M., 1998. Impact of climatic changes on the benthic foraminiferal fauna in the Ionian Sea during the last 330,000 years. *Paleoceanography* 13, 447–458. <https://doi.org/10.1029/98PA01864>.
- Schmiedl, G., Mitschele, A., Beck, S., Emeis, K.-C., Hemleben, C., Schulz, H., Sperling, M., Weldeab, S., 2003. Benthic foraminiferal record of ecosystem variability in the eastern Mediterranean Sea during times of sapropel S5 and S6 deposition. *Palaeogeogr. Palaeoclimatol. Palaeoecol.* 190, 139–164. [https://doi.org/10.1016/S0031-0182\(02\)00603-X](https://doi.org/10.1016/S0031-0182(02)00603-X).
- Schmiedl, G., Kuhnt, T., Ehrmann, W., Emeis, K.-C., Hamann, Y., Kotthoff, U., Dulski, P., Pross, J., 2010. Climatic forcing of eastern Mediterranean deep-water formation and benthic ecosystems during the past 22 000 years. *Quat. Sci. Rev.* 29, 3006–3020. <https://doi.org/10.1016/j.quascirev.2010.07.002>.
- Shackleton, N.J., Hall, M.A., Vincent, E., 2000. Phase relationships between millennial-scale events 64,000–24,000 years ago. *Paleoceanography* 15, 565–569. <https://doi.org/10.1029/2000PA000513>.
- Sierro, F.J., Andersen, N., 2022. An exceptional record of millennial-scale climate variability in the southern Iberian Margin during MIS 6: Impact on the formation of sapropel S6. *Quat. Sci. Rev.* 286, 107527 <https://doi.org/10.1016/j.quascirev.2022.107527>.
- Stanley, D.J., Maldonado, A., Stuckenrath, R., 1975. Strait of Sicily depositional rates and patterns, and possible reversal of currents in the late Quaternary. *Palaeogeogr. Palaeoclimatol. Palaeoecol.* 18, 279–291. [https://doi.org/10.1016/0031-0182\(75\)90037-1](https://doi.org/10.1016/0031-0182(75)90037-1).
- Stocker, T.F., Johnsen, S.J., 2003. A minimum thermodynamic model for the bipolar seesaw. *Paleoceanography* 18. <https://doi.org/10.1029/2003PA000920>.
- Tachikawa, K., Vidal, L., Cornuault, M., Garcia, M., Pothin, A., Sonzogni, C., Bard, E., Menot, G., Revel, M., 2015. Eastern Mediterranean Sea circulation inferred from the conditions of S1 sapropel deposition. *Clim. Past* 11, 855–867. <https://doi.org/10.5194/cp-11-855-2015>.
- Ten Haven, H.L., 1986. Organic and Inorganic Geochemical Aspects of Mediterranean Late Quaternary Sapropels and Messinian Evaporitic Deposits. Instituut voor Aardwetenschappen der Rijksuniversiteit te Utrecht.
- Thirumalai, K., Quinn, T.M., Marino, G., 2016. Constraining past seawater  $\delta^{18}\text{O}$  and temperature records developed from foraminiferal geochemistry. *Paleoceanography* 31, 1409–1422. <https://doi.org/10.1002/2016PA002970>.
- Thunell, R.C., Williams, D.F., 1989. Glacial–Holocene salinity changes in the Mediterranean Sea: hydrographic and depositional effects. *Nature* 338, 493–496. <https://doi.org/10.1038/338493a0>.
- Thunell, R.C., Williams, D.F., Kennett, J.P., 1977. Late Quaternary paleoclimatology, stratigraphy and sapropel history in eastern Mediterranean deep-sea sediments. *Mar. Micropaleontol.* 2, 371–388. [https://doi.org/10.1016/0377-8398\(77\)90018-4](https://doi.org/10.1016/0377-8398(77)90018-4).
- Thunell, R.C., Williams, D.F., Cita, M.B., 1983. Glacial anoxia in the eastern Mediterranean. *J. Foraminiferal Res.* 13, 283–290. <https://doi.org/10.2113/gsfjr.13.4.283>.
- Tierney, J.E., Lewis, S.C., Cook, B.I., LeGrande, A.N., Schmidt, G.A., 2011. Model, proxy and isotopic perspectives on the East African Humid Period. *Earth Planet. Sci. Lett.* 307, 103–112. <https://doi.org/10.1016/j.epsl.2011.04.038>.
- Tierney, J.E., Pausata, F.S.R., deMenocal, P.B., 2017. Rainfall regimes of the Green Sahara. *Sci. Adv.* 3, e1601503 <https://doi.org/10.1126/sciadv.1601503>.
- Tolderlund, D.S., 1971. Distribution and ecology of living planktonic foraminifera in surface waters of the Atlantic and Indian Oceans. *Micropaleontol. OCEANS* 105–149.
- Toledo, F.A., Cachão, M., Costa, K.B., Pivel, M.A., 2007. Planktonic foraminifera, calcareous nannoplankton and ascidian variations during the last 25 kyr in the Southwestern Atlantic: a paleoproductivity signature? *Mar. Micropaleontol.* 64, 67–79.
- Toucanne, S., Zaragosi, S., Bourillet, J.-F., Cremer, M., Eynaud, F., van Vliet-Lanoë, B., Pénaud, A., Fontanier, C., Turon, J.L., Cortijo, E., 2009. Timing of massive ‘Fleuve Manche’ discharges over the last 350 kyr: insights into the European ice-sheet oscillations and the European drainage network from MIS 10 to 2. *Quat. Sci. Rev.* 28, 1238–1256. <https://doi.org/10.1016/j.quascirev.2009.01.006>.
- Toucanne, S., Minto'o, C.M.A., Fontanier, C., Bassetti, M.-A., Jorjy, S.J., Jouet, G., 2015. Tracking rainfall in the northern Mediterranean borderlands during sapropel deposition. *Quat. Sci. Rev.* 129, 178–195.
- Triantaphyllou, M.V., Antonarakou, A., Kouli, K., Dimiza, M., Kontakiotis, G., Papanikolaou, M.D., Ziveri, P., Mortyn, P.G., Lianou, V., Lykousis, V., Dermizakis, M.D., 2009. Late Glacial–Holocene ecostratigraphy of the south-eastern Aegean Sea, based on plankton and pollen assemblages. *Geo-Mar. Lett.* 29, 249–267. <https://doi.org/10.1007/s00367-009-0139-5>.
- Triantaphyllou, M.V., Antonarakou, A., Dimiza, M., Anagnostou, C., 2010. Calcareous nannofossil and planktonic foraminiferal distributional patterns during deposition of sapropels S6, S5 and S1 in the Libyan Sea (Eastern Mediterranean). *Geo-Mar. Lett.* 30, 1–13. <https://doi.org/10.1007/s00367-009-0145-7>.
- Van Santvoort, P.J.M., De Lange, G.J., Thomson, J., Cussen, H., Wilson, T.R.S., Krom, M. D., Ströhle, K., 1996. Active post-depositional oxidation of the most recent sapropel (S1) in sediments of the eastern Mediterranean Sea. *Geochim. Cosmochim. Acta* 60, 4007–4024. [https://doi.org/10.1016/S0016-7037\(96\)00253-0](https://doi.org/10.1016/S0016-7037(96)00253-0).
- Van Straaten, L., 1972. Holocene stages of oxygen depletion in deep waters of the Adriatic Sea. *Mediterranean Sea* 631–643.
- Van Straaten, L., 1966. Micro-malacological Investigation of Cores from Southeastern Adriatic Sea. Koninklijke Nederlandse Akademie Van Wetenschappen-Proceedings Series b-Physical Sciences, 69, p. 429.
- Vergnaud-Grazzini, C., 1985. Mediterranean late Cenozoic Stable Isotope Record: Stratigraphic and Paleoclimatic Implications. In: Stanley, D.J., Wezel, F.-C. (Eds.), *Geological Evolution of the Mediterranean Basin*. Springer, New York, New York, NY, pp. 413–451. [https://doi.org/10.1007/978-1-4613-8572-1\\_20](https://doi.org/10.1007/978-1-4613-8572-1_20).
- Vergnaud-Grazzini, C., Ryan, W.B., Cita, M.B., 1977. Stable isotopic fractionation, climate change and episodic stagnation in the eastern Mediterranean during the late Quaternary. *Mar. Micropaleontol.* 2, 353–370. [https://doi.org/10.1016/0377-8398\(77\)90017-2](https://doi.org/10.1016/0377-8398(77)90017-2).
- Violanti, D., Grecchi, G., Castradori, D., 1991. Paleoenvironmental interpretation of Core BAN88-11GC (Eastern Mediterranean, Pleistocene–Holocene), on the grounds of Foraminifera, Thecosoma and Calcareous Nannofossils. *Il Quaternario* 4, 13–39.
- Wagner, B., Vogel, H., Francke, A., Friedrich, T., Donders, T., Lacey, J.H., Leng, M.J., Regattieri, E., Sadori, L., Wilke, T., 2019. Mediterranean winter rainfall in phase with African monsoons during the past 1.36 million years. *Nature* 573, 256–260. <https://doi.org/10.1038/s41586-019-1529-0>.
- Wainer, K., Genty, D., Blamart, D., Bar-Matthews, M., Quinif, Y., Plagnes, V., 2013. Millennial climatic instability during penultimate glacial period recorded in a South-Western France speleothem. *Palaeogeogr. Palaeoclimatol. Palaeoecol.* 376, 122–131. <https://doi.org/10.1016/j.palaeo.2013.02.026>.
- Wang, Y., Cheng, H., Edwards, R.L., Kong, X., Shao, X., Chen, S., Wu, J., Jiang, X., Wang, X., An, Z., 2008. Millennial-and orbital-scale changes in the East Asian monsoon over the past 224,000 years. *Nature* 451, 1090–1093. <https://doi.org/10.1038/nature06692>.
- Wegwerth, A., Dellwig, O., Kaiser, J., Ménot, G., Bard, E., Shumilovskikh, L., Schnetger, B., Kleinhanns, I.C., Wille, M., Arz, H.W., 2014. Meltwater events and the Mediterranean reconnection at the Saalian–Eemian transition in the Black Sea. *Earth Planet. Sci. Lett.* 404, 124–135.
- Wegwerth, A., Dellwig, O., Wulf, S., Plessen, B., Kleinhanns, I.C., Nowaczyk, N.R., Jiabo, L., Arz, H.W., 2019. Major hydrological shifts in the Black Sea “Lake” in response to ice sheet collapses during MIS 6 (130–184 ka BP). *Quat. Sci. Rev.* 219, 126–144. <https://doi.org/10.1016/j.quascirev.2019.07.008>.
- Wegwerth, A., Kaiser, J., Dellwig, O., Arz, H.W., 2020. Impact of Eurasian Ice Sheet and North Atlantic climate dynamics on Black Sea Temperature Variability during the Penultimate Glacial (MIS 6, 130–184 ka BP). *Paleoceanog. Paleoclimatol.* 35 <https://doi.org/10.1029/2020PA003882>.
- Williams, D.F., Thunell, R.C., 1979. Faunal and oxygen isotopic evidence for surface water salinity changes during sapropel formation in the eastern Mediterranean. *Sediment. Geol.* 23, 81–93. [https://doi.org/10.1016/0037-0738\(79\)90007-1](https://doi.org/10.1016/0037-0738(79)90007-1).
- Williams, D.F., Thunell, R.C., Kennett, J.P., 1978. Periodic Freshwater Flooding and Stagnation of the Eastern Mediterranean Sea during the late Quaternary. *Science* 201, 252–254. <https://doi.org/10.1126/science.201.4352.252>.
- Williams, G.L., Damassa, S.P., Fensome, R.A., Guerstein, G.R., 2017. A response to ‘Comment to Wetzeliella and its allies – the “hole” story: a taxonomic revision of the Paleogene dinoflagellate subfamily Wetzelielloideae by Williams et al. (2015)’. *Palynology* 41, 430–437. <https://doi.org/10.1080/01916122.2017.1283367>.
- Wilson, G.P., Frogley, M.R., Hughes, P.D., Roucoux, K.H., Margari, V., Jones, T.D., Leng, M.J., Tzedakis, P.C., 2021. Persistent millennial-scale climate variability in Southern Europe during Marine Isotope Stage 6. *Quatern. Sci. Adv.* 3, 100016 <https://doi.org/10.1016/j.qsa.2020.100016>.
- Winter, A., 1994. Biogeography of living coccolitho-hores in ocean waters. *Coccolithophores* 161–177.
- Wood, G.D., 1996. Palynological techniques-processing and microscopy. In: Jasonius, J., McGregor, D.C. (Eds.), *Palynology: Principles and Application*, 1. American Association of Stratigraphic Palynologists Foundation, pp. 29–50.
- Wright, R.C., Hay, W.W., Jones, J.L., Bock, W.D., 1971. The abundance and distribution of foraminifera in a back-reef environment, Molasses Reef, Florida. *Miami Geol. Soc. Mem.* 1, 121–174.
- Young, J.R., Geisen, M., Cros, L., Kleijne, A., Sprengel, C., Probert, I., Østergaard, J., 2003. A guide to extant coccolithophore taxonomy. *J. Nannoplankton Res.* 1, 1–132. <https://doi.org/10.58998/jnr2297>. Special Issue.
- Ziegler, M., Tüenter, E., Lourens, L.J., 2010. The precession phase of the boreal summer monsoon as viewed from the eastern Mediterranean (ODP Site 968). *Quat. Sci. Rev.* 29, 1481–1490. <https://doi.org/10.1016/j.quascirev.2010.03.011>.
- Zirks, E., Krom, M.D., Zhu, D., Schmiedl, G., Goodman-Tchernov, B.N., 2019. Evidence for the Presence of Oxygen-Depleted Sapropel Intermediate Water across the Eastern Mediterranean during Sapropel S1. *ACS Earth Space Chem.* 3, 2287–2297. <https://doi.org/10.1021/acsearthspacechem.9b00128>.
- Ziveri, P., Thunell, R.C., Rio, D., 1995. Export production of coccolithophores in an upwelling region: results from San Pedro Basin, Southern California Borderlands. *Mar. Micropaleontol.* 24, 335–358. [https://doi.org/10.1007/978-3-662-06278-4\\_15](https://doi.org/10.1007/978-3-662-06278-4_15).
- Ziveri, P., Baumann, K.-H., Böckel, B., Bollmann, J., Young, J.R., 2004. Biogeography of selected Holocene coccoliths in the Atlantic Ocean. In: Thierstein, H.R., Young, J.R. (Eds.), *Coccolithophores*. Springer, Berlin Heidelberg, Berlin, Heidelberg, pp. 403–428. [https://doi.org/10.1007/978-3-662-06278-4\\_15](https://doi.org/10.1007/978-3-662-06278-4_15).
- Zonneveld, K.A., Marret, F., Versteegh, G.J., Bogus, K., Bonnet, S., Bouimetarhan, I., Crouch, E., de Vernal, A., Elshanawany, R., Edwards, L., 2013. Atlas of modern dinoflagellate cyst distribution based on 2405 data points. *Rev. Palaeobot. Palynol.* 191, 1–197.
- Zwief, K.L., Hennekam, R., Donders, T.H., Van Helmond, N.A., De Lange, G.J., Sangiorgi, F., 2018. Marine productivity, water column processes and seafloor anoxia in relation to Nile discharge during sapropels S1 and S3. *Quat. Sci. Rev.* 200, 178–190. <https://doi.org/10.1016/j.quascirev.2018.08.026>.